

Solvent-Induced Negative Energetic Elasticity in a Lattice Polymer Chain

Nobu C. Shirai^{1,*} and Naoyuki Sakumichi^{2,†}

¹Center for Information Technologies and Networks, Mie University, Tsu, Mie 514-8507, Japan

²Graduate School of Engineering, The University of Tokyo,
7-3-1 Hongo, Bunkyo-ku, Tokyo 113-8656, Japan

(Dated: March 20, 2023)

The negative internal energetic contribution to the elastic modulus (negative energetic elasticity) has been recently observed in polymer gels. This finding challenges the conventional notion that the elastic moduli of rubberlike materials are determined mainly by entropic elasticity. However, the microscopic origin of negative energetic elasticity has not yet been clarified. Here, we consider the n -step interacting self-avoiding walk on a cubic lattice as a model of a single polymer chain (a subchain of a network in a polymer gel) in a solvent. We theoretically demonstrate the emergence of negative energetic elasticity based on an exact enumeration up to $n = 20$ and analytic expressions for arbitrary n in special cases. Furthermore, we demonstrate that the negative energetic elasticity of this model originates from the attractive polymer–solvent interaction, which locally stiffens the chain and conversely softens the stiffness of the entire chain. This model qualitatively reproduces the temperature dependence of negative energetic elasticity observed in the polymer-gel experiments, indicating that the analysis of a single chain can explain the properties of negative energetic elasticity in polymer gels.

Since the widespread acceptance of the macromolecular hypothesis [1], the entropic elasticity originating from flexible polymer chains in rubberlike materials has been investigated experimentally and theoretically [2–4]. The simplest theoretical explanations for entropic elasticity are provided by statistical models of ideal chains. For example, the random walk, freely jointed chain, and freely rotating chain models are described in textbooks on statistical mechanics [5, 6], polymer physics [7, 8], and soft matter physics [9].

Rubberlike materials composed of polymer chains exhibit an interplay between entropic (G_S) and energetic (G_U) contributions to the elastic modulus ($G = G_S + G_U$). In the case of conventional natural and synthetic rubbers, $|G_U|$ is significantly smaller than G_S [2–4]. A small $|G_U|$ is considered to originate from the conformational change of polymer chains, which has been theoretically modeled such as the rotational isometric state model [10]. By contrast, the significant negative G_U was recently observed in a chemically crosslinked polymer gel, i.e., a polymer network containing a large amount of solvent [11–13]. In this observation, $|G_U|$ is significantly larger than that of the energetic elasticity originating from conformational changes, and $|G_U|$ reaches the same order of magnitude as G , as shown in Fig. 1(a).

Although two previous studies [11, 13] measured the shear modulus G over a narrow temperature (T) range where G can be approximated as a linear function of T , the combination of both results shows that G is an increasing convex function of T , as shown in Fig. 1(a). Here, T dependence of G is fitted by quadratic function (black solid curve), and the tangent of the fitted curve (dotted line) at the reference temperature $T^* = 293$ K intersects with the horizontal axis at T_U^* and vertical axis at G_U^* . These two experiments had the same conditions,

excluding the temperature ranges; Ref. [11] used $T = 278$ – 298 K, whereas Ref. [13] used $T = 288$ – 308 K. By shifting T^* from 288 (Ref. [11]) to 298 K (Ref. [13]), the values of T_U^* increased. These results imply that (i) G is an increasing convex function of T , (ii) T_U^* depends on the

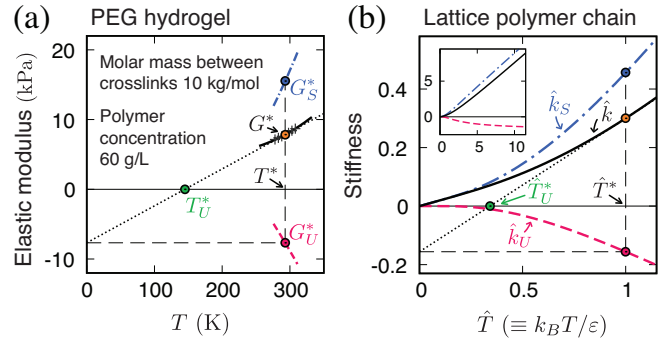


FIG. 1. Experimental results for a polymer gel [11, 13] and theoretical results of the lattice polymer chain model. (a) Temperature dependence of shear modulus G of poly(ethylene glycol) (PEG) hydrogel for $T = 278$ – 308 K, including the midpoint $T^* = 293$ K [seven points, including the orange point (G^*) in the center]. These data are obtained from Refs. [11, 13]. The black solid curve is the fitted quadratic function of these points. The dotted line is the tangent of the solid curve at the reference temperature T^* , which intersects with the horizontal axis at T_U^* (> 0) and the vertical axis at G_U^* (< 0). Temperature dependencies of G_U (pink dashed curve) and G_S (blue dot-dashed curve) are calculated from the fitted quadratic function. (b) Temperature dependence of stiffness (\hat{k}) of lattice polymer chain model for $(n, r) = (20, 10a)$ and its energetic (\hat{k}_U) and entropic (\hat{k}_S) contributions. The tangent (dotted line) of \hat{k} at \hat{T}^* intersects with the horizontal axis at \hat{T}_U^* (> 0) and vertical axis at $\hat{k}_U^* \equiv \hat{k}_U(r, \hat{T}^*)$ (< 0).

reference temperature T^* , and (iii) G_U is a monotonically decreasing function of T .

In this Letter, focusing on a subchain (i.e., a chain between adjacent crosslinks) in the polymer network of polymer gels, we theoretically demonstrate the emergence of negative energetic elasticity in a single polymer chain model on a lattice. Notably, the previous experimental studies [11, 13] show that G is described as $G = a(T - T_U^*)$ in a narrow temperature range, where a depends on the polymer network topology, but T_U^* does not [see Eqs. (7) and (9) in Ref. [12]]. Thus, network topology does not contribute to the proportion of energetic elasticity to entropic elasticity ($G_U^*/G_S^* = -T_U^*/T^*$), suggesting that a subchain is sufficient to investigate G_U^*/G_S^* . As shown in Figs. 1(a) and 1(b), this polymer chain model explains G_U as a monotonically decreasing function of temperature in polymer gel experiments. Furthermore, we provide a microscopic mechanism for the emergence of negative energetic elasticity by examining the polymer-solvent interaction strength in this model.

Lattice polymer chain model.—We consider a single polymer chain model surrounded by solvent molecules on a simple cubic lattice (three dimensions). This model was first introduced by Orr for highly dilute polymer solutions [14] and is one of the simplest ways to express the interaction between a polymer chain and solvent molecules. In Figs. 2(a) and 2(b), we use a square lattice (two dimensions) for illustration. As indicated in Fig. 2(a), this model consists of solvent molecules and a polymer chain represented by an n -step self-avoiding walk (SAW) [15], which has n bonds connecting $n + 1$ consecutive and distinct lattice sites (i.e., the polymer segments). The energy function of the model is given by

$$E(\omega) = \varepsilon_{pp}m_{pp}(\omega) + \varepsilon_{ps}m_{ps}(\omega) + \varepsilon_{ss}m_{ss}(\omega), \quad (1)$$

where ω denotes the configuration of SAWs, and $m_{pp}(\omega)$, $m_{ps}(\omega)$, and $m_{ss}(\omega)$ are the numbers of the polymer-polymer, polymer-solvent, and solvent-solvent contact pairs, respectively. Here, the interaction energies acting between each pair are ε_{pp} , ε_{ps} , and ε_{ss} , respectively. In Eq. (1), we do not consider the bending energetic terms, which are essential for semiflexible polymers [16], to focus on the solvent-induced energetic elasticity.

Once the entire lattice size is given, the total number of contact pairs, $m_{pp}(\omega) + m_{ps}(\omega) + m_{ss}(\omega)$, is constant. In addition, we derive $2m_{pp}(\omega) + m_{ps}(\omega) = (z - 2)n + z$ by counting solvent molecules surrounding ω . Here, z is the coordination number of a lattice, e.g., $z = 4$ and 6 for the square and cubic lattices, respectively. Thus, when n is constant, Eq. (1) is rewritten [9, 14] as

$$E(\omega) = \varepsilon m(\omega), \quad (2)$$

where a constant term has been omitted, and $\varepsilon \equiv \varepsilon_{pp} - 2\varepsilon_{ps} + \varepsilon_{ss}$ and $m(\omega) \equiv m_{pp}(\omega)$. Here, the original model

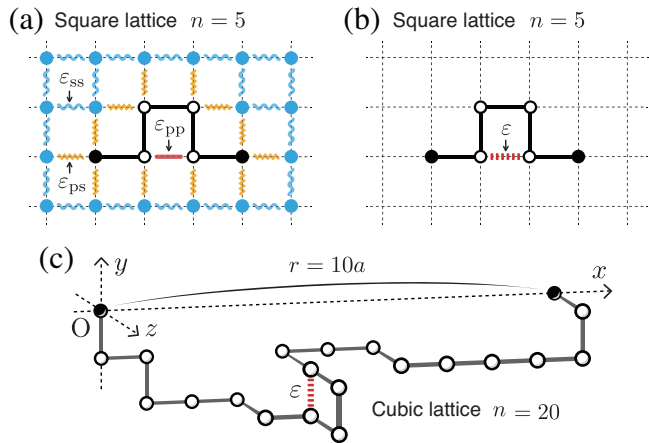


FIG. 2. (a) Two-component model of single polymer chain (open and filled black circles connected with lines) and solvent molecules (light-blue filled circles) on square lattice. There are three types of nearest-neighbor interactions. (b) Reduced model mathematically equivalent to (a). (c) Example of interacting self-avoiding walk on cubic lattice with on-axis constraint on end-to-end vector.

illustrated in Fig. 2(a) was reduced to the so-called interacting SAW [17] shown in Fig. 2(b), which is a single-chain system with the intrachain interaction. The interacting SAW reduces to the (noninteracting) SAW at $\varepsilon = 0$. Notably, many studies on the interacting SAW have focused on the self-attractive condition ($\varepsilon < 0$) to investigate the collapsing transition [18–22]. By contrast, this study focuses mainly on the self-repulsive condition ($\varepsilon > 0$) to investigate the effect of attractive polymer-solvent interactions.

Energetic and entropic elasticities in lattice polymer chain.—To calculate the stiffness (a single-chain counterpart of the elastic modulus) of the lattice polymer chain model, we impose an on-axis constraint on the end-to-end vector of ω . Here, the length of the vector is r , and the direction of the vector is the same as the x axis, as shown in Fig. 2(c). The partition function with the on-axis constraint using Eq. (2) is given by

$$Z(r, T) = \sum_{m=0}^{m_{ub}} W_{n,m}(r) e^{-\varepsilon m/(k_B T)}, \quad (3)$$

where k_B is the Boltzmann constant, T is the absolute temperature, and $W_{n,m}(r)$ is the number of possible ω for a given set of n , r , and m . In Eq. (3), m_{ub} is an upper bound of m summation [i.e., $W_{n,m}(r) = 0$ for $m \geq m_{ub} + 1$], which is discussed in Supplemental Material, Sec. S1 [23]. The corresponding free energy is $A(r, T) = -k_B T \ln Z(r, T)$.

We define the stiffness of the lattice polymer chain model with the on-axis constraint. In the continuum limit ($n \rightarrow \infty$ and lattice spacing $a \rightarrow 0$), the stiffness is

defined as the second derivative of the free energy:

$$k(r, T) \equiv \frac{\partial^2 A(r, T)}{\partial r^2} = k_B T \left[\left(\frac{\partial Z(r, T)}{\partial r} \right)^2 - \frac{\partial^2 Z(r, T)}{\partial r^2} \right]. \quad (4)$$

Thus, we define the finite difference form of stiffness as

$$k(r, T) \equiv k_B T \left[\left(\frac{1}{Z(r, T)} \sum_{m=0}^{m_{\text{ub}}} \frac{\Delta W_{n,m}(r)}{\Delta r} e^{-\varepsilon m/(k_B T)} \right)^2 - \frac{1}{Z(r, T)} \sum_{m=0}^{m_{\text{ub}}} \frac{\Delta^2 W_{n,m}(r)}{\Delta r^2} e^{-\varepsilon m/(k_B T)} \right], \quad (5)$$

where the first- and second-order differences of $W_{n,m}(r)$ are given by $\Delta W_{n,m}(r) \equiv [W_{n,m}(r + \Delta r) - W_{n,m}(r - \Delta r)]/2$, and $\Delta^2 W_{n,m}(r) \equiv W_{n,m}(r + \Delta r) - 2W_{n,m}(r) + W_{n,m}(r - \Delta r)$, respectively. Here, $\Delta r \equiv 2a$ because ω exists only for odd $\hat{r} \equiv r/a$ for odd n and only for even \hat{r} for even n (see Supplemental Material, Sec. S11 [23]).

We decompose the elasticity into its energetic and entropic contributions as $k = k_U + k_S$ in the same way as in Refs. [11, 12]. According to thermodynamics, $A = U - TS$, where U is the internal energy, and S is the entropy. Thus, in the continuum limit, the energetic and entropic contributions are $k_U(r, T) \equiv \partial^2 U(r, T)/\partial r^2$ and $k_S(r, T) \equiv -T\partial^2 S(r, T)/\partial r^2$, respectively. From Maxwell's relation, we have $k_S(r, T) = T\partial k(r, T)/\partial T$. Thus, we calculate $k_S(r, T) = T\partial k(r, T)/\partial T$ and $k_U = k - k_S$ in the lattice polymer chain model using Eq. (5).

Exact enumeration and derivation of polynomial functions.—We exactly enumerate $W_{n,m}(r)$ for $1 \leq n \leq 20$ using the simplest recursive algorithm [27] with two pruning algorithms, considering the octahedral symmetry of the simple cubic lattice and the reachability of ω to a specific endpoint (see Supplemental Material, Sec. S2 [23]). The complete lists of $W_{n,m}(r)$ are provided in Sec. S11 of Supplemental Material [23]. Those lists are consistent with the results reported in Refs. [14, 28–37] (see Supplemental Material, Sec. S3 [23]). Using the lists of $W_{n,m}(r)$ with additional results up to $n = 26$ for $r = (n - 8)a$, we exactly derive the polynomial functions $W_{n,m}((n - 2)a)$, $W_{n,m}((n - 4)a)$, $W_{n,m}((n - 6)a)$, and $W_{n,m}((n - 8)a)$ for arbitrary integers n and m , which are provided in Sec. S12 of SM [23].

Emergence of negative energetic elasticity.—From the lists of $W_{n,m}(r)$, we can analytically calculate k , k_U , and k_S . Figure 1(b) shows a representative result for $\varepsilon > 0$ and $(n, r) = (20, 10a)$. Here, we introduce the dimensionless quantities $\hat{k} \equiv a^2 k/\varepsilon$, $\hat{k}_U \equiv a^2 k_U/\varepsilon$, $\hat{k}_S \equiv a^2 k_S/\varepsilon$, and $\hat{T} \equiv k_B T/\varepsilon$. Figure 1(b) demonstrates the emergence of the solvent-induced negative energetic elasticity ($k_U < 0$) in the model. Figure 2(c) displays an example of ω for $r = 10a$. In this Letter, we use $r = 10a$ for the illustration [e.g., Fig. 1(b)] because the maximum value

of $|k_U|/k$ is larger than $r \neq 10a$. Although the extent of k_U/k depends on r , the negative k_U can be observed for different $n \geq 6$ and r . Notably, we find that $k_U < 0$ for arbitrary $n \geq 13$, $\varepsilon > 0$, and positive finite T using the polynomial functions $W_{n,m}((n - 2)a)$, $W_{n,m}((n - 4)a)$, $W_{n,m}((n - 6)a)$, and $W_{n,m}((n - 8)a)$ (see Supplemental Material, Sec. S13 [23]).

Figures 1(a) and (b) demonstrate the qualitative consistency between the previous experimental results for the shear modulus G of the poly(ethylene glycol) (PEG) hydrogel [11, 13] and our results. These results suggest that negative energetic elasticity ($G_U < 0$) in the polymer gel originates from a single chain ($k_U < 0$).

To examine the effect of the sign of ε on the energetic elasticity, we show the dependence of the stiffness $\hat{k}/\hat{T} = a^2 k/(k_B T)$ on $1/\hat{T} \equiv \varepsilon/(k_B T)$ in Fig. 3. [Note that $\hat{k} \rightarrow \infty$ and $\hat{k}_S \rightarrow \infty$ at $\varepsilon = 0$ (noninteracting SAW), whereas $0 < \hat{k}/\hat{T} < \infty$ and $0 < \hat{k}_S/\hat{T} < \infty$.] Figure 3 depicts that the energetic contributions are negative, zero, and positive for $\varepsilon > 0$, $\varepsilon = 0$, and $\varepsilon < 0$, respectively, for $(n, r) = (20, 10a)$.

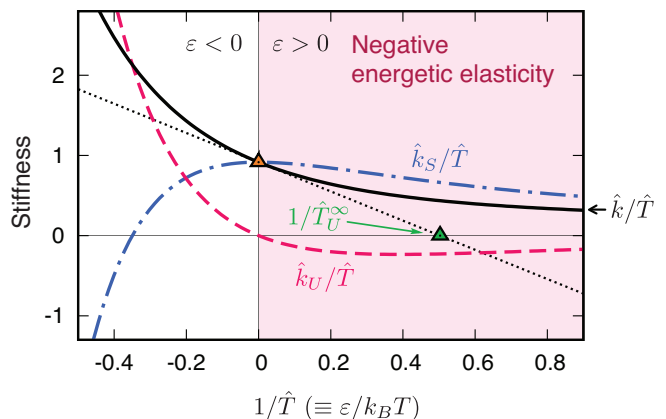


FIG. 3. Analytic curves of \hat{k}/\hat{T} , \hat{k}_U/\hat{T} , and \hat{k}_S/\hat{T} as functions of $1/\hat{T}$ for $(n, r) = (20, 10a)$. The tangent (dotted line) of \hat{k}/\hat{T} at $1/\hat{T}^* = 0$ intersects with the horizontal axis at $1/\hat{T}^\infty$. The condition for negative energetic elasticity ($\hat{k}_U/\hat{T} < 0$) is $\varepsilon > 0$.

As depicted in Fig. 1(b), $\hat{T}_U^* \equiv \hat{T}_U(\hat{T}^*)$ denotes the \hat{T} intercept of the tangent of $\hat{k} = \hat{k}(\hat{T})$ at the reference temperature $\hat{T} = \hat{T}^*$. For polymer gels, T_U^* [Fig. 1(a)] is a key factor in the analysis of negative energetic elasticity because T_U^* does not depend on the polymer network topology [11, 12]. In addition, in the lattice polymer chain model, T_U^* is a better measure of the negative energetic elasticity than k_U , because $T_U^* = \varepsilon \hat{T}_U^*/k_B$ is independent of the lattice spacing a , unlike $k_U = \varepsilon \hat{k}_U/a^2$, which depends on a .

We define $\hat{T}_U^\infty \equiv \lim_{\hat{T}^* \rightarrow \infty} \hat{T}_U(\hat{T}^*)$, which is a good indicator of the negative energetic elasticity in the sense that $\hat{T}_U^\infty > 0$ is identical to $\hat{k}_U < 0$ in the case of $\varepsilon > 0$.

As shown in Fig. 3, the $1/\hat{T}$ intercept of the tangent of \hat{k}/\hat{T} at $1/\hat{T} = 0$ corresponds to $1/\hat{T}_V^\infty$. Notably, \hat{T}_V^∞ is a functional of $W_{n,m}(r)$ and is a rational number for a given set of n , r , and m (see Supplemental Material, Secs. S5, S6, and S7 [23]). In Fig. 4(a), we plot \hat{T}_V^∞ that is

$$\hat{T}_V^\infty(n, (n-2)a) = \frac{4(15n^8 - 356n^7 + 3766n^6 - 23016n^5 + 88019n^4 - 213804n^3 + 317784n^2 - 256008n + 81484)}{(n-1)(9n^8 - 204n^7 + 2026n^6 - 11648n^5 + 42733n^4 - 102444n^3 + 156272n^2 - 137656n + 53028)}. \quad (6)$$

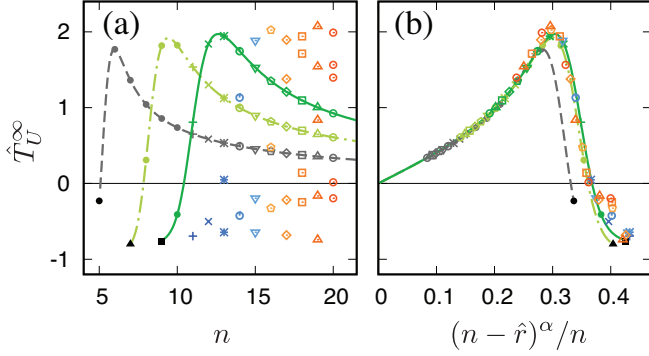


FIG. 4. (a) Exact values of $\hat{T}_V^\infty(n, r)$ for $n = 5, 6, \dots, 20$ and three analytic curves for $r = (n-2)a$, $(n-4)a$, and $(n-6)a$, shown as gray dashed, light-green dot-dashed, and green solid curves, respectively. (b) Same points and curves are plotted as functions of $(n - \hat{r})^\alpha/n$, where $\alpha = 3/4$. These collapse onto a single master curve.

The other rational functions, $\hat{T}_V^\infty(n, (n-4)a)$ and $\hat{T}_V^\infty(n, (n-6)a)$, are provided in Sec. S15 of Supplemental Material [23]. In Fig. 4(a), we overlay the three curves of these functions, which pass through all the corresponding points of \hat{T}_V^∞ .

Figure 4(b) shows \hat{T}_V^∞ as a function of $(n - \hat{r})^\alpha/n$ for $\alpha = 3/4$. Here, the three curves of the analytic expressions and the points collapse onto a single master curve, except for the small values of n . A possible origin of the exponent $\alpha = 3/4$ is the reduction of the dimensionality from three to two by the on-axis constraint on the end-to-end vector, resulting in the universal critical exponent $\nu = 3/4$ of the two-dimensional SAW [38, 39] (see Supplemental Material, Sec. S8 [23]).

Microscopic mechanism of negative energetic elasticity.—To characterize the microscopic properties of the lattice polymer chain model with a negative k_U , we evaluate the thermal average of the mean free path of the interacting SAW as

$$\ell(r, T) = \frac{1}{Z(r, T)} \sum_{m=0}^{m_{ub}} \sum_{b=0}^{n-1} \frac{na}{b+1} W_{n,m,b}(r) e^{-\varepsilon m/(k_B T)}, \quad (7)$$

calculated from $W_{n,m}(r)$ (the exact rational numbers of \hat{T}_V^∞ are listed in Sec. S14 of Supplemental Material [23]).

We successfully determine the analytic expressions of \hat{T}_V^∞ as the rational functions of n for $r = (n-2)a$, $(n-4)a$, and $(n-6)a$, using the polynomial functions of $W_{n,m}(r)$. For example,

where b is the number of bending points of ω , and $W_{n,m,b}(r)$ is the number of ω for a given set of n , r , m , and b . In Eq. (7), $na/(b+1)$ is the mean free path for each ω (see Supplemental Material, Sec. S9 [23]). For example, $b = 4$ and 13 for ω in Figs. 2(b) and 2(c), respectively.

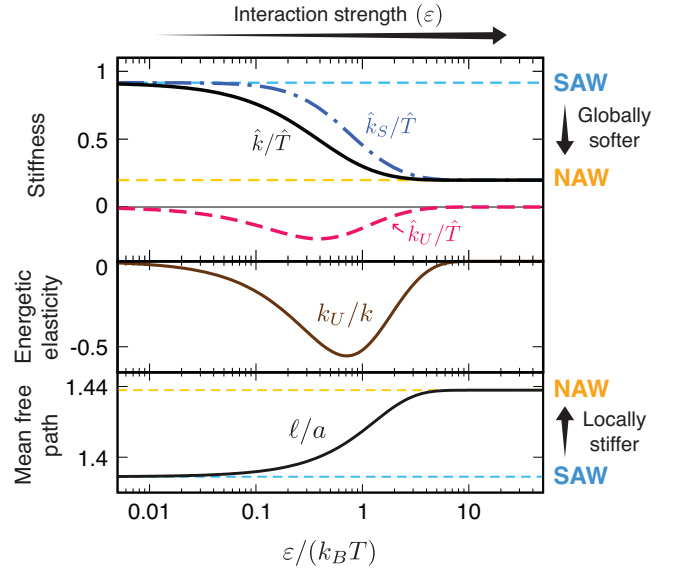


FIG. 5. Polymer-solvent interaction $[\varepsilon/(k_B T)]$ dependences of \hat{k}/\hat{T} , \hat{k}_U/\hat{T} , \hat{k}_S/\hat{T} (top panel), k_U/k (middle panel), and ℓ/a (bottom panel) for $(n, r) = (20, 10a)$ and $\varepsilon > 0$. As ε increases, the lattice polymer chain model (i.e., interacting SAW) becomes globally softer and locally stiffer.

Figure 5 indicates that $\hat{k}/\hat{T} = a^2 k/(k_B T)$ increases with $\varepsilon/(k_B T)$, whereas ℓ decreases with $\varepsilon/(k_B T)$. Here, \hat{k}/\hat{T} characterizes the “global” stiffness of the whole polymer chain, whereas ℓ characterizes the “local” stiffness of the chain. Thus, the global and local stiffnesses are negatively correlated, which is also observed in various sets of (n, r) (see Supplemental Material, Sec. S4 [23]). These results confirm that polymer chains become locally stiffer because of the attractive interaction with solvent molecules, and globally softer because of the smaller curvature of free energy in the case of $\varepsilon > 0$ and $\hat{k}_U < 0$.

This is the microscopic mechanism of negative energetic elasticity in the lattice polymer chain model.

Figure 5 also shows values corresponding to the SAW ($\varepsilon \rightarrow 0$) and neighbor-avoiding walk (NAW; $\varepsilon \rightarrow \infty$) [32, 40, 41] (see Supplemental Material, Sec. S10 [23]). The emergence of negative energetic elasticity is characterized by the crossover between the SAW and NAW, which only possess entropic elasticity. The minimum of k_U/k is -0.554 at $\varepsilon/(k_B T) \simeq 0.712$, where the interaction strength ε is the same order of magnitude as the thermal energy $k_B T$.

Concluding remarks.—We used the simplest lattice polymer chain model to explain both the energetic and entropic elasticities (Fig. 2). By exactly enumerating the configurations of this model, we obtained the stiffness of the chain and its energetic and entropic contributions (Fig. 3). This result demonstrates that the negative energetic elasticity originates from the polymer–solvent interaction. The three rational functions of T_U^∞ with respect to n are derived from the enumeration results (Fig. 4), revealing that negative energetic elasticity exists for all finite $n \geq 6$. We revealed a negative correlation between the stiffness of the whole polymer chain and the mean free path of the chain (Fig. 5). In short, locally stiffer chains are globally softer.

Although this simple model does not include chemical details, it qualitatively reproduces the temperature dependence of negative energetic elasticity observed in the experiments conducted on the PEG hydrogel [11, 13] (Fig. 1). This fact indicates that negative energetic elasticity would emerge in various single polymer chains [42–44] and various polymer gels other than the PEG hydrogel. Therefore, this model provides a starting point for the further understanding of negative energetic elasticity in polymer chains and networks in solvents.

We thank Yuki Yoshikawa and Takamasa Sakai for allowing us to use the experimental data in Fig. 1(a) and for their useful comments, especially those regarding the temperature dependence of T_U^* . This study was supported by JSPS KAKENHI Grant No. 22K13973 to N.C.S., and No. 19K14672 and No. 22H01187 to N.S.

* These authors contributed equally; Corresponding author. shirai@cc.mie-u.ac.jp

† These authors contributed equally; Corresponding author. sakumichi@tetrapod.t.u-tokyo.ac.jp

- [1] H. Staudinger, Über polymerisation, Ber. Dtsch. Chem. Ges. **53**, 1073 (1920).
- [2] K. H. Meyer and C. Ferri, Sur l'élasticité du caoutchouc, Helv. Chim. Acta **18**, 570 (1935).
- [3] R. L. Anthony, R. H. Caston, and E. Guth, Equations of state for natural and synthetic rubber-like materials. I. Unaccelerated natural soft rubber, J. Phys. Chem. **46**, 826 (1942).
- [4] J. E. Mark, Thermoelastic results on rubberlike networks and their bearing on the foundations of elasticity theory, J. Polym. Sci. **11**, 135 (1976).
- [5] C. Kittel, *Thermal Physics* (Wiley, New York, 1969)
- [6] H. B. Callen, *Thermodynamics and an Introduction to Thermostatistics* (Wiley, New York, 1991).
- [7] P. G. de Gennes, *Scaling Concepts in Polymer Physics* (Cornell University Press, Ithaca, 1979).
- [8] M. Rubinstein and R. H. Colby, *Polymer Physics* (Oxford University Press, Oxford, 2003).
- [9] M. Doi, *Soft Matter Physics* (Oxford University Press, Oxford, 2013).
- [10] P. J. Flory, *Statistical Mechanics of Chain Molecules* (Wiley Interscience, New York, 1969).
- [11] Y. Yoshikawa, N. Sakumichi, U. Chung, and T. Sakai, Negative Energy Elasticity in a Rubberlike Gel, Phys. Rev. X **11**, 011045 (2021).
- [12] N. Sakumichi, Y. Yoshikawa, and T. Sakai, Linear elasticity of polymer gels in terms of negative energy elasticity, Polym. J. **53**, 1293 (2021).
- [13] T. Fujiyabu, T. Sakai, R. Kudo, Y. Yoshikawa, T. Katashima, U. Chung, and N. Sakumichi, Temperature Dependence of Polymer Network Diffusion, Phys. Rev. Lett. **127**, 237801 (2021).
- [14] W. J. Orr, Statistical treatment of polymer solutions at infinite dilution, Trans. Faraday Soc. **43**, 12 (1947).
- [15] N. Madras and G. Slade, *The Self-Avoiding Walk*, Probability and Its Applications (Birkhäuser, Boston, 1996).
- [16] C. P. Broedersz and F. C. MacKintosh, Modeling semiflexible polymer networks, Rev. Mod. Phys. **86**, 995 (2014).
- [17] C. Vanderzande, *Lattice Models of Polymers*, Cambridge Lecture Notes in Physics (Cambridge University Press, Cambridge, England, 1998).
- [18] D. C. Rapaport, On the polymer phase transition, Phys. Lett. **48A**, 339 (1974).
- [19] D. Marenduzzo, A. Maritan, A. Rosa, and F. Seno, Stretching of a Polymer Below the θ Point, Phys. Rev. Lett. **90**, 088301 (2003).
- [20] S. Kumar, I. Jensen, J. L. Jacobsen, and A. J. Guttman, Role of Conformational Entropy in Force-Induced Biopolymer Unfolding, Phys. Rev. Lett. **98**, 128101 (2007).
- [21] J. H. Lee, S. Y. Kim, and J. Lee, Exact partition function zeros of a polymer on a simple cubic lattice, Phys. Rev. E **86**, 011802 (2012).
- [22] Y. H. Hsieh, C. N. Chen, and C. K. Hu, Efficient algorithm for computing exact partition functions of lattice polymer models, Comput. Phys. Commun. **209**, 27 (2016).
- [23] See Supplemental Material for (i) details of the enumeration method, (ii) derivations of analytic expressions, (iii) discussion on the data collapse shown in Fig. 4(b), and (iv) complete lists of enumeration data, which includes Refs. [24–26].
- [24] R. D. Schram, G. T. Barkema, and R. H. Bisseling, Exact enumeration of self-avoiding walks, J. Stat. Mech. (2011) P06019.
- [25] R. D. Schram, G. T. Barkema, and R. H. Bisseling, SAW-doubler: A program for counting self-avoiding walks, Comput. Phys. Commun. **184**, 891 (2013).
- [26] N. Clisby, R. Liang, and G. Slade, Self-avoiding walk enumeration via the lace expansion, J. Phys. A **40**, 10973 (2007).

- [27] J. L. Martin, The exact enumeration of self-avoiding walks on a lattice, *Math. Proc. Cambridge Philos. Soc.* **58**, 92 (1962).
- [28] M. E. Fisher and M. F. Sykes, Excluded-volume problem and the Ising model of ferromagnetism, *Phys. Rev.* **114**, 45 (1959).
- [29] M. F. Sykes, Some counting theorems in the theory of the Ising model and the excluded volume problem, *J. Math. Phys.* **2**, 52 (1961).
- [30] M. F. Sykes, Self-avoiding walks on the simple cubic lattice, *J. Chem. Phys.* **39**, 410 (1963).
- [31] M. E. Fisher and B. J. Hiley, Configuration and free energy of a polymer molecule with solvent interaction, *J. Chem. Phys.* **34**, 1253 (1961).
- [32] A. M. Nemirovsky, K. F. Freed, T. Ishinabe, and J. F. Douglas, Marriage of exact enumeration and 1/d expansion methods: Lattice model of dilute polymers, *J. Stat. Phys.* **67**, 1083 (1992).
- [33] P. Butera and M. Comi, Critical specific heats of the N-vector spin models on the simple cubic and bcc lattices, *Phys. Rev. B* **60**, 6749 (1999).
- [34] A. J. Guttmann, On the critical behaviour of self-avoiding walks, *J. Phys. A* **20**, 1839 (1987).
- [35] C. Domb, J. Gillis, and G. Wilmers, On the shape and configuration of polymer molecules, *Proc. Phys. Soc. London* **85**, 625 (1965).
- [36] N. J. A. Sloane, Entry A001412 in The On-Line Encyclopedia of Integer Sequences, <https://oeis.org/A001412> (2022).
- [37] J. Myers, Entry A174319 in The On-Line Encyclopedia of Integer Sequences, <https://oeis.org/A174319> (2022).
- [38] B. Nienhuis, Exact Critical Point and Critical Exponents of $O(n)$ Models in Two Dimensions, *Phys. Rev. Lett.* **49**, 1062 (1982).
- [39] B. Nienhuis, Critical behavior of two-dimensional spin models and charge asymmetry in the Coulomb gas, *J. Stat. Phys.* **34**, 731 (1984).
- [40] G. Torrie and S. G. Whittington, Exact enumeration of neighbour-avoiding walks on the tetrahedral and body-centred cubic lattices, *J. Phys. A* **8**, 1178 (1975).
- [41] T. Ishinabe and Y. Chikahisa, Exact enumerations of self-avoiding lattice walks with different nearest-neighbor contacts, *J. Chem. Phys.* **85**, 1009 (1986).
- [42] K. Nakajima, H. Watabe, and T. Nishi, Single polymer chain rubber elasticity investigated by atomic force microscopy, *Polymer* **47**, 2505 (2006).
- [43] A. Kolberg, C. Wenzel, K. Hackenstrass, R. Schwarzl, C. Rüttiger, T. Hugel, M. Gallei, R. R. Netz, and B. N. Balzer, Opposing temperature dependence of the stretching response of single PEG and PNIPAM polymers, *J. Am. Chem. Soc.* **141**, 11603 (2019).
- [44] Y. Bao, Z. Luo, and S. Cui, Environment-dependent single-chain mechanics of synthetic polymers and biomacromolecules by atomic force microscopy-based single-molecule force spectroscopy and the implications for advanced polymer materials, *Chem. Soc. Rev.* **49**, 2799 (2020).

Supplemental Material for: “Solvent-Induced Negative Energetic Elasticity in a Lattice Polymer Chain”

Nobu C. Shirai^{1,*} and Naoyuki Sakumichi^{2,†}

¹Center for Information Technologies and Networks, Mie University, Tsu, Mie 514-8507, Japan

²Graduate School of Engineering, The University of Tokyo,
7-3-1 Hongo, Bunkyo-ku, Tokyo 113-8656, Japan

(Dated: March 20, 2023)

S1. UPPER BOUND OF CONTACT PAIRS

We consider an upper bound of the number of nearest-neighbor contact pairs m , which is a non-negative integer, for a configuration ω of n -step SAW. Notably, the number of segments of the lattice polymer chain is $n + 1$. First, we give a loose upper bound of m from a fully packed ω without vacant sites inside, which was derived by Orr [S1]. The maximum number of contacts for the two segments at both ends of the lattice polymer chain is $z - 1$, where z is the coordination number of a lattice, and that for the other $n - 1$ segments other than both ends is $z - 2$. Thus, we obtain an upper bound of m as

$$\begin{aligned} m_{\text{ub}}^{\text{Orr}} &= \frac{2(z-1) + (n-1)(z-2)}{2} \\ &= \left(\frac{z}{2} - 1\right)n + \frac{z}{2}, \end{aligned} \quad (\text{S1})$$

where we divide by the factor two not to doubly count the pairs shared by two segments.

Second, we reduce the upper bound of m by considering segments on the surface of the fully packed ω . For $n = 0$ and 1, the upper bound $m_{\text{ub}} = 0$ because ω does not have sufficient length to make a contact. For $n \geq 2$, the upper bound becomes

$$m_{\text{ub}} = m_{\text{ub}}^{\text{Orr}} - z = \left(\frac{z}{2} - 1\right)n - \frac{z}{2}, \quad (\text{S2})$$

because at least one polymer segment exists on the surface of ω for each direction, which cannot maximize the number of contacts. In the case of a simple cubic lattice, the upper bound is $m_{\text{ub}} = 2n - 3$ because $z = 6$.

S2. TWO PRUNING ALGORITHMS OF ENUMERATION METHOD

This section explains the details of the two pruning algorithms of the enumeration method.

The first algorithm prunes the search tree based on the symmetry of ω on a lattice (e.g., see Sec. 2.2 of Ref. [S2]).

We select a single configuration from the set of ω , which is generated by symmetry operations including rotation and mirroring. We multiply the symmetry factor of the selected ω by its number and prune the search tree for the other members of the set.

The second algorithm prunes the search tree based on the reachability of ω to a given endpoint. This algorithm requires the specification of an endpoint for ω . To calculate $W_n(r)$ or $W_{n,m}(r)$, we specify the endpoint at $(r, 0, 0)$. We calculate the shortest path length to the endpoint and compare it with the number of remaining steps of the recursion. When the shortest path length exceeds the number of remaining steps, we terminate further search for the branch.

Notably, the enumeration data might be extended using the enumeration techniques developed during the last couple of decades for the (noninteracting) SAW [S3–S5]. However, those techniques were never extended to the interacting SAW, and additional efforts are required to store contact information [S2].

S3. VALIDATION OF ENUMERATION RESULTS

This section explains the validation of the enumeration results. We validate the result of $W_n(a)$ in Tables S1 and S2 using data in Ref. [S6] up to $n = 20$, and validate the result of $W_{13}(r)$ for $r = a, 3a, \dots, 13a$ in Table S1 using data in Ref. [S7].

To indirectly validate the result of $W_{n,m}(r)$, we also use the results for the number of n -step SAWs (without the constraint on the end-to-end vector), c_n , and the number of these walks for a given number of m , $c_n(m)$, which can be calculated using only the first algorithm. Here, c_n and $c_n(m)$ satisfy

$$c_n = \sum_{m=0}^{m_{\text{ub}}} c_n(m). \quad (\text{S3})$$

The values of c_n that we obtained are validated by Ref. [S1] up to $n = 6$, by Ref. [S8] up to $n = 9$, by Ref. [S9] up to $n = 10$, by Ref. [S10] up to $n = 14$, and by Refs. [S11, S12] up to $n = 18$. Notably, the values of c_{11} in Ref. [S9] and c_{16} in Ref. [S10] are inconsistent with the ones in Refs. [S11, S12], which are latest and more reliable. The values of $c_n(m)$ obtained in this study were validated by the numbers in Ref. [S1] up to $n = 6$, those

* These authors contributed equally; Corresponding author. shirai@cc.mie-u.ac.jp

† These authors contributed equally; Corresponding author. sakumichi@tetrapod.t.u-tokyo.ac.jp

of $c_n(0)$ by Ref. [S13] up to $n = 9$, and those of $c_n(m)$ for $m \leq 5$ by Ref. [S14] up to $n = 11$. Notably, the value of $c_{10}(0)$ in Ref. [S13] is inconsistent with those reported in Refs. [S14, S15], which are latest and more reliable.

S4. POLYMER-SOLVENT INTERACTION DEPENDENCIES OF STIFFNESS AND ENERGETIC ELASTICITY

This section describes the polymer-solvent interaction (ε) dependencies of \hat{k}/\hat{T} , k_U/k , and ℓ for $\varepsilon > 0$ and various lengths n . Here, we denote $\hat{T} \equiv k_B T/\varepsilon$.

Figures S1(a,b) reveal the $\varepsilon/(k_B T)$ dependence of \hat{k}/\hat{T} for all possible r of $n = 10$ and 20 ($\varepsilon > 0$). The curves of $r \geq 6a$ for $n = 10$ and $r \geq 8a$ for $n = 20$ reveal a monotonic decrease in \hat{k}/\hat{T} with $\varepsilon/(k_B T)$, i.e.,

$$\frac{\partial(\hat{k}/\hat{T})}{\partial[\varepsilon/(k_B T)]} < 0, \quad (\text{S4})$$

whereas the curves for $(n, r) = (10, 4a)$, $(20, 4a)$, and $(20, 6a)$ have increasing and decreasing regions of \hat{k}/\hat{T} . Figure S1(c) shows the $\varepsilon/(k_B T)$ dependence of \hat{k}/\hat{T} for larger n ($n = 40$ and 80) with $r = (n-2)a$, $(n-4)a$, and $r = (n-6)a$, which are exactly calculated using the polynomial functions $W_{n,m}((n-2)a)$, $W_{n,m}((n-4)a)$, and $W_{n,m}((n-6)a)$ given in Sec. S12. These curves monotonically decrease with $\varepsilon/(k_B T)$.

The regions of Eq. (S4) correspond to those of $\hat{k}_U < 0$ because

$$\frac{\partial(\hat{k}/\hat{T})}{\partial[\varepsilon/(k_B T)]} = \frac{\partial(\hat{k}/\hat{T})}{\partial(1/\hat{T})} = \hat{k} - \hat{k}_S = \hat{k}_U, \quad (\text{S5})$$

where we used $\varepsilon/(k_B T) \equiv 1/\hat{T}$, and Eqs. (S8) and (S9). Equation (S5) means that \hat{k}/\hat{T} decreases when \hat{k}_U is negative.

Figures S1(d,e) show the $\varepsilon/(k_B T)$ dependence of k_U/k for all possible r of $n = 10$ and 20 ($\varepsilon > 0$). Notably, the sign of k_U is the same as that of k_U/k because $k > 0$ for $\varepsilon/(k_B T) > 0$ from our observation. The curves of $r \geq 6a$ for $n = 10$ and $r \geq 8a$ for $n = 20$ exhibit $k_U < 0$ for a positive finite $\varepsilon/(k_B T)$, i.e., $0 < \varepsilon/(k_B T) < \infty$, whereas the curves for $(n, r) = (10, 4a)$, $(20, 4a)$, and $(20, 6a)$ have the positive and negative regions of k_U .

Figure S1(f) depicts the $\varepsilon/(k_B T)$ dependence of k_U/k for larger n ($n = 40$ and 80) with $r = (n-2)a$, $(n-4)a$, and $r = (n-6)a$, which are exactly calculated using the polynomial functions $W_{n,m}((n-2)a)$, $W_{n,m}((n-4)a)$, and $W_{n,m}((n-6)a)$ given in Sec. S12. The sign of k_U is always negative for a positive finite $\varepsilon/(k_B T)$ [$0 < \varepsilon/(k_B T) < \infty$] in each pair of (n, r) .

In Sec. S13, we demonstrate that (i) $\hat{k}_U((n-2)a, \hat{T}) < 0$ for $n \geq 7$ and positive finite \hat{T} (i.e., $0 < \hat{T} < \infty$), (ii) $\hat{k}_U((n-4)a, \hat{T}) < 0$ for $n \geq 10$ and positive finite \hat{T} , and (iii) $\hat{k}_U((n-6)a, \hat{T}) < 0$ for $n \geq 13$ and positive finite \hat{T} .

Thus, the lattice polymer chain model (interacting SAW) always exhibits negative energetic elasticity for $n \geq 13$ and positive finite \hat{T} , at least, around the fully stretched conditions [i.e., $r = (n-2)a$, $(n-4)a$, and $(n-6)a$].

Figure S1(g) shows the dependencies of ℓ on $\varepsilon/(k_B T)$ of all possible r for $n = 10$ and 20 . For $(n, r) = (10, 10a)$ and $(20, 20a)$, both ℓ remain at $10a$ and $20a$, respectively, independent of $\varepsilon/(k_B T)$, because the fully stretched ω is only allowed. For $(n, r) = (10, 2a)$ – $(10, 8a)$ and $(20, 2a)$ – $(20, 18a)$, ℓ monotonically increases with $\varepsilon/(k_B T)$ and converges to finite values in the SAW and NAW limits. As indicated in Fig. S1(h), the differences of ℓ between the NAW and SAW limits ($\ell_{\text{NAW}} - \ell_{\text{SAW}}$) are positive, except for the fully stretched conditions, i.e., $(n, r) = (10, 10a)$ and $(20, 20a)$, for which the values are zero.

When $\hat{k}_U = \frac{\partial(\hat{k}/\hat{T})}{\partial[\varepsilon/(k_B T)]} < 0$ [Eq. (S5)], ℓ and \hat{k}/\hat{T} are negatively correlated because ℓ monotonically increases with $\varepsilon/(k_B T)$ and \hat{k}/\hat{T} monotonically decreases with $\varepsilon/(k_B T)$.

The variance and standard deviation of the mean free path ℓ are defined by

$$V_\ell \equiv \frac{1}{Z} \sum_{m=0}^{m_{\text{ub}}} \sum_{b=0}^{n-1} \left(\frac{na}{b+1} \right)^2 W_{n,m,b}(r) e^{-\varepsilon m/(k_B T)} - \ell^2, \\ \sigma_\ell \equiv V_\ell^{\frac{1}{2}}, \quad (\text{S6})$$

where ℓ is given by Eq. (7) in the main text. The middle panel of Fig. S1(i) shows the $\varepsilon/(k_B T)$ dependence of σ_ℓ for $(n, r) = (20, 10a)$ and $\varepsilon > 0$. σ_ℓ increases with $\varepsilon/(k_B T)$, ranging from $0.175a$ to $0.193a$. Because $\ell_{\text{NAW}} - \ell_{\text{SAW}} \simeq 0.049a$ in Fig. S1(h), the standard deviation of the mean free path ℓ is 3–4 times longer than $\ell_{\text{NAW}} - \ell_{\text{SAW}}$. Thus, a larger effort is required to experimentally observe the negative correlation between ℓ and \hat{k}/\hat{T} in a single polymer chain. However, it might be observed in a polymer gel because it is composed of a large number of polymer chains.

The top and bottom panels of Fig. S1(i) shows the $\varepsilon/(k_B T)$ dependence of σ_ℓ of all possible r for $n = 10$ and 20 , respectively. σ_ℓ increases with $\varepsilon/(k_B T)$ for all r , except $(n, r) = (10, 10a)$ and $(20, 20a)$ because the fully stretched ω is only allowed in this condition.

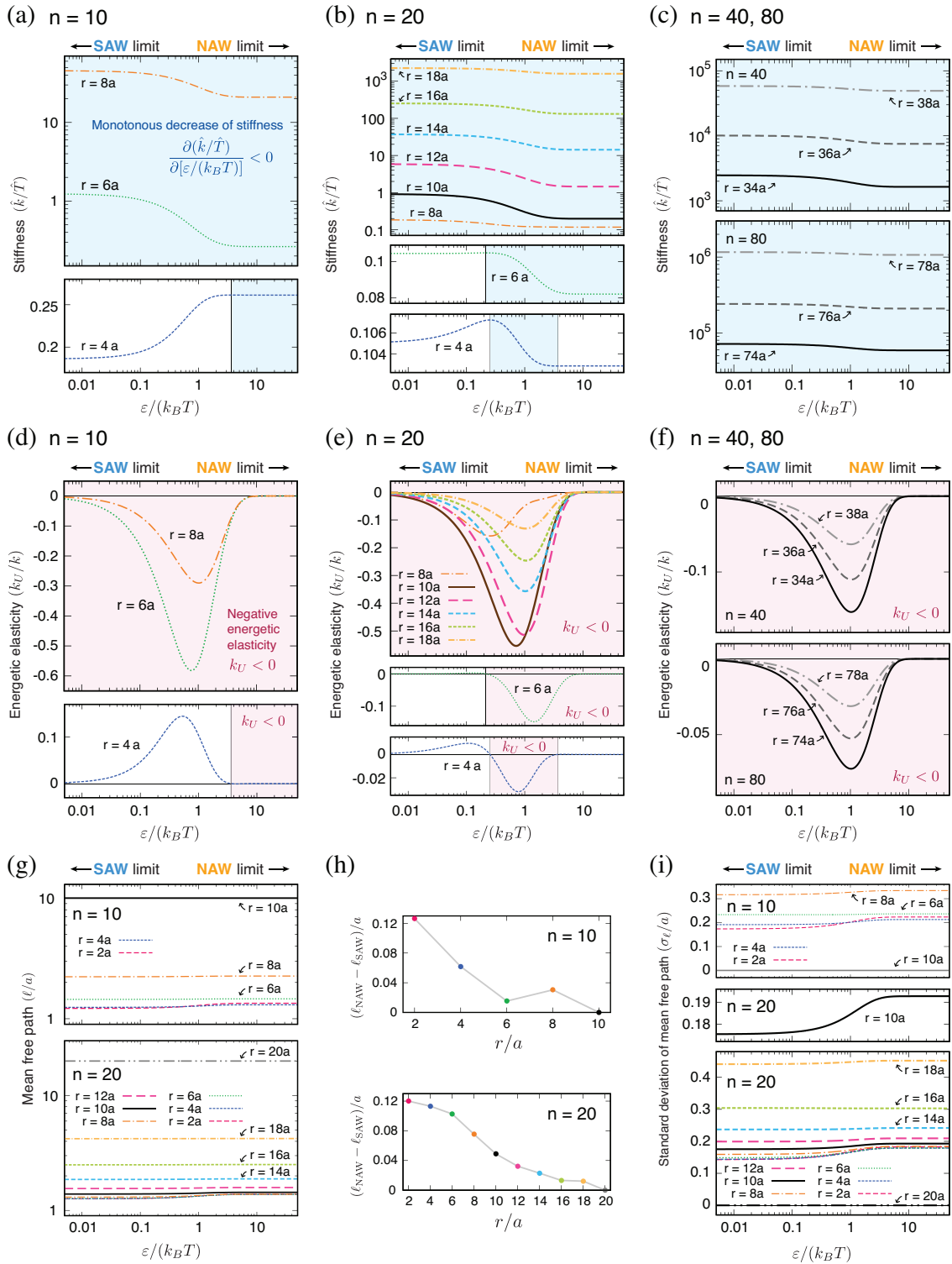


FIG. S1. (a–f) Polymer–solvent interaction $[\varepsilon/(k_B T)]$ dependences of (a,b,c) stiffness (\hat{k}/\hat{T}) and (d,e,f) negative energetic elasticity k_U/k for $\varepsilon > 0$ in the logarithmic scale. We show (a,d) $n = 10$, (b,e) $n = 20$, and (c,f) $n = 40$ and 80 . Curves for all possible r are shown in (a), (b), (d), and (e), whereas curves for $r = (n - 2)a$, $(n - 4)a$, and $(n - 6)a$ are shown in (c) and (f). The light-blue regions in (a), (b), and (c) exhibit the monotonically decreasing regions of \hat{k}/\hat{T} , i.e., $\partial(\hat{k}/\hat{T})/\partial[\varepsilon/(k_B T)] < 0$. The pink regions in (d), (e), and (f) display negative energetic elasticity, i.e., $k_U < 0$, which correspond to the light-blue regions in (a), (b), and (c), respectively, because of Eq. (S5). (g) Dependence of ℓ/a on $\varepsilon/(k_B T)$ for $(n, r) = (10, 2a)–(10, 10a)$ (top panel) and $(n, r) = (20, 2a)–(20, 20a)$ (bottom panel). (h) end-to-end distance (r/a) dependence of $(\ell_{NAW} - \ell_{SAW})/a$ for $(n, r) = (10, 2a)–(10, 10a)$ (top panel) and $(n, r) = (20, 2a)–(20, 20a)$ (bottom panel). (i) Dependence of σ_ℓ/a on $\varepsilon/(k_B T)$ for $(n, r) = (10, 2a)–(10, 10a)$ (top panel), for $(n, r) = (20, 10a)$ (middle panel), and $(n, r) = (20, 2a)–(20, 20a)$ (bottom panel). Scales in the bottom panels of (a) and (b) and in all panels of (c) and (g) are double logarithmic scales.

where

$$\begin{aligned}
Z_\infty &\equiv \lim_{\hat{T} \rightarrow \infty} Z(r, \hat{T}) = \sum_{m=0}^{m_{\text{ub}}} W_{n,m}(r), \\
Z'_\infty &\equiv \lim_{\hat{T} \rightarrow \infty} Z'(r, \hat{T}) = - \sum_{m=0}^{m_{\text{ub}}} m W_{n,m}(r), \\
\Delta Z_\infty &\equiv \lim_{\hat{T} \rightarrow \infty} \Delta Z(r, \hat{T}) = \sum_{m=0}^{m_{\text{ub}}} \Delta W_{n,m}(r), \\
\Delta^2 Z_\infty &\equiv \lim_{\hat{T} \rightarrow \infty} \Delta^2 Z(r, \hat{T}) = \sum_{m=0}^{m_{\text{ub}}} \Delta^2 W_{n,m}(r), \\
\Delta Z'_\infty &\equiv \lim_{\hat{T} \rightarrow \infty} \Delta Z'(r, \hat{T}) = - \sum_{m=0}^{m_{\text{ub}}} m \Delta W_{n,m}(r), \\
\Delta^2 Z'_\infty &\equiv \lim_{\hat{T} \rightarrow \infty} \Delta^2 Z'(r, \hat{T}) = - \sum_{m=0}^{m_{\text{ub}}} m \Delta^2 W_{n,m}(r).
\end{aligned}$$

Because $W_{n,m}(r)$, $\Delta W_{n,m}(r)$, $\Delta^2 W_{n,m}(r)$, and m are rational numbers, $\hat{k}_U^\infty(r)$ is a rational number for a given set of n and r . Moreover,

$$\begin{aligned}
\lim_{\hat{T} \rightarrow \infty} \frac{\partial \hat{k}(r, \hat{T})}{\partial \hat{T}} &= \lim_{\hat{T} \rightarrow \infty} \frac{\hat{k}_S(r, \hat{T})}{\hat{T}} \\
&= \left(\frac{\Delta Z_\infty}{Z_\infty \Delta \hat{r}} \right)^2 - \frac{\Delta^2 Z_\infty}{Z_\infty \Delta \hat{r}^2}, \quad (\text{S16})
\end{aligned}$$

is a rational number for a given set of n and r . Using Eqs. (S11), (S15), and (S16), we obtain $\hat{T}_U^\infty(n, r)$ as a functional of $W_{n,m}(r)$:

$$\hat{T}_U^\infty(n, r) = \frac{2\Delta Z_\infty (\Delta Z_\infty Z'_\infty - Z_\infty \Delta Z'_\infty) + Z_\infty (Z_\infty \Delta^2 Z'_\infty - \Delta^2 Z_\infty Z'_\infty)}{(\Delta Z_\infty)^2 Z_\infty - Z_\infty^2 \Delta^2 Z_\infty}, \quad (\text{S17})$$

which is a rational number for a given set of n and r .

S8. DISCUSSION ON DATA COLLAPSE

In this section, we discuss the physical interpretation of the data collapse shown in Fig. 4 (b) in the main text. We discuss the newly found scaling relation followed by the rescaling of ε in the continuum limit ($n \rightarrow \infty$ and $a \rightarrow 0$).

A. Scaling relation between n and $s \equiv n - \hat{r}$

We explain the scaling relation found in the data collapse shown in Fig. 4 (b) in the main text. For a lattice polymer chain with n steps with the end-to-end distance r , at least $\hat{r} \equiv r/a$ steps are taken for the $+x$ -direction and the rest steps are $s \equiv n - \hat{r}$. Some of s steps are taken for the $\pm y$ - and $\pm z$ -directions to go away from and come back to the x -axis. In this sense, s is the amount of slack in the chain. By using s , the horizontal axis of Fig. 4 (b) can be written as $(n - \hat{r})^\alpha / n = s^\alpha / n$.

From the data collapse shown in Fig. 4 (b), we observed the scaling relation between two pairs of n and s

$$s' = \left(\frac{n'}{n} \right)^{\frac{1}{\alpha}} s, \quad (\text{S18})$$

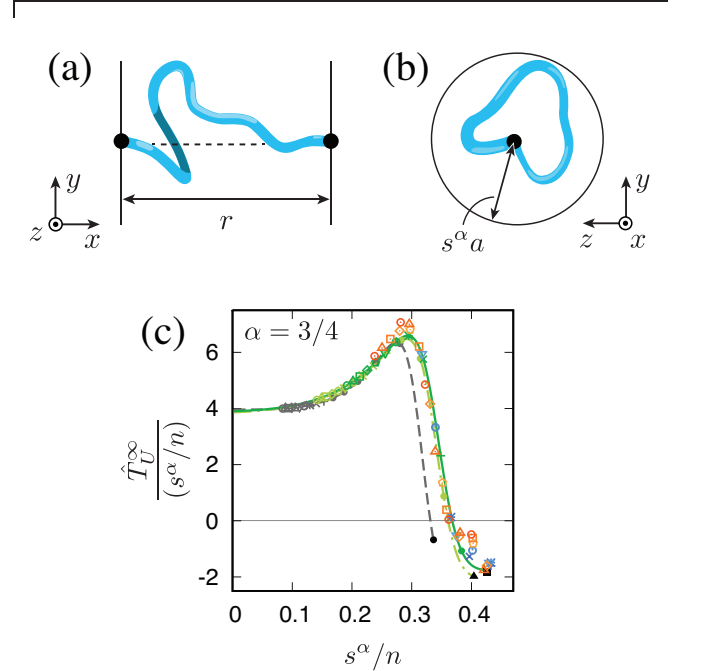


FIG. S3. (a,b) Two views of a polymer chain on a three-dimensional space. (c) Rescaled plot of Fig. 4 (b) in the main text, to have a finite value of \hat{T}_U^∞ in the continuum limit ($n \rightarrow \infty$ and $a \rightarrow 0$).

where $\alpha = 3/4$, which is the same as the universal critical exponent $\nu = 3/4$ of the two-dimensional SAW [S16, S17]. Equation (S18) gives s' for n' -step

chain to have the same \hat{T}_U^∞ as a chain with n and s . Figures S3(a) and (b) illustrates a possible scenario to explain the origin of the critical exponent in a two-dimensional space ($\alpha = 3/4$) as follows. The on-axis constraint on the end-to-end vector reduces the effective dimensionality from three to two, and $s^\alpha a$, which contains the amount of chain slack s , gives typical length scale of the radius on the yz -plane.

The scaling relation in Eq. (S18) can also be interpreted such that the sets of (n, r) which have the same value of s^α/n have the same values of \hat{T}_U^∞ . For example, the sets $(n, r) = (17, 9a)$ and $(20, 10a)$ that have almost the same values of $s^\alpha/n = (n - \hat{r})^\alpha/n \simeq 0.28$ give the almost the same values of \hat{T}_U^∞ as

$$\begin{aligned}\hat{T}_U^\infty(17, 9a) &= \frac{3527424314659253062003}{1862575181539491665133} \simeq 1.89, \\ \hat{T}_U^\infty(20, 10a) &= \frac{2060069205296200981486403946}{1035875167962083022664474501} \simeq 1.99,\end{aligned}$$

where the rational numbers are taken from Table S22 in Sec. S14.

B. Rescaling of ε in the continuum limit

We discuss the rescaling of ε proportional to n to have the finite value of T_U^∞ in the continuum limit ($n \rightarrow \infty$ and $a \rightarrow 0$). In this limit, $s^\alpha/n = (n - \hat{r})^\alpha/n \rightarrow 0$ and thus $\hat{T}_U^\infty = k_B T_U^\infty / \varepsilon \rightarrow 0$ [see Fig. 4 (b) in the main text]. However, assuming that the interaction energy ε changes with n as $\varepsilon \propto n$, the value of $T_U^\infty = \varepsilon \hat{T}_U^\infty / k_B$ can be rescued to be finite positive as shown in Fig. S3 (c).

Furthermore, we discuss the rescaling of ε by using the rational functions given in Eqs. (S106)–(S108) in Sec. S15. The Taylor expansions of these functions by $1/n$ are given by

$$\hat{T}_U^\infty(n, (n-2)a) = \frac{20}{3n} + O\left(\frac{1}{n^2}\right), \quad (\text{S19})$$

$$\hat{T}_U^\infty(n, (n-4)a) = \frac{164}{15n} + O\left(\frac{1}{n^2}\right), \quad (\text{S20})$$

$$\hat{T}_U^\infty(n, (n-6)a) = \frac{524}{35n} + O\left(\frac{1}{n^2}\right). \quad (\text{S21})$$

The leading terms of Eqs. (S19)–(S21) are in the first order of $1/n$. Thus, by multiplying the left-hand sides of Eqs. (S19)–(S21) by n and taking the limit of $n \rightarrow \infty$, we obtain the following finite positive values:

$$\lim_{n \rightarrow \infty} n \hat{T}_U^\infty(n, (n-2)a) = \frac{20}{3}, \quad (\text{S22})$$

$$\lim_{n \rightarrow \infty} n \hat{T}_U^\infty(n, (n-4)a) = \frac{164}{15}, \quad (\text{S23})$$

$$\lim_{n \rightarrow \infty} n \hat{T}_U^\infty(n, (n-6)a) = \frac{524}{35}. \quad (\text{S24})$$

These results suggest that $T_U^\infty = \varepsilon \hat{T}_U^\infty / k_B$ converges to a positive finite value if we assume $\varepsilon \propto n$.

By defining a rescaled interaction energy as $\varepsilon' \equiv \varepsilon s^\alpha / n$ where $0 < \varepsilon' < \infty$, we obtain

$$\begin{aligned}\frac{k_B}{\varepsilon'} T_U^\infty(n, (n-2)a) &= \frac{n}{2^\alpha} \hat{T}_U^\infty(n, (n-2)a) \\ &= \frac{20}{3 \cdot 2^\alpha} + O\left(\frac{1}{n}\right), \quad (\text{S25})\end{aligned}$$

$$\begin{aligned}\frac{k_B}{\varepsilon'} T_U^\infty(n, (n-4)a) &= \frac{n}{4^\alpha} \hat{T}_U^\infty(n, (n-4)a) \\ &= \frac{164}{15 \cdot 4^\alpha} + O\left(\frac{1}{n}\right), \quad (\text{S26})\end{aligned}$$

$$\begin{aligned}\frac{k_B}{\varepsilon'} T_U^\infty(n, (n-6)a) &= \frac{n}{6^\alpha} \hat{T}_U^\infty(n, (n-6)a) \\ &= \frac{524}{35 \cdot 6^\alpha} + O\left(\frac{1}{n}\right). \quad (\text{S27})\end{aligned}$$

In the limit of $n \rightarrow \infty$ with $\alpha = 3/4$, the right-hand sides of Eqs. (S25)–(S27) converge to $20/(3 \cdot 2^\alpha) \simeq 3.96$, $164/(15 \cdot 4^\alpha) \simeq 3.87$, and $524/(35 \cdot 6^\alpha) \simeq 3.91$, respectively. These values correspond to the $[\hat{T}_U^\infty/(s^\alpha/n)]$ -intercepts of the curves in Fig. S3 (c). We expect that $k_B T_U^\infty(n, r)/\varepsilon'$ converges to a single value ($\simeq 3.9$) independent of the value of r in the continuum limit, which means that negative energetic elasticity exists even in the continuum limit. The rescaling of ε is expected to be explained by using the renormalization group with simultaneously changing the length scale (a) and coupling constant (ε).

S9. EXAMPLE OF MEAN FREE PATH

Using the example configuration ω for $(n, r) = (7, 3a)$ shown in Fig. S4, we explain the thermal average of mean free path of the interacting SAW, $\ell(r, \hat{T})$, which is defined as Eq. (7) in the main text. In this configuration ω , the number of bending points $b(\omega)$ is four. The number of straight paths between two bending points (between \odot and \odot) and between an endpoint and a bending point (between \odot and \bullet) is $b(\omega) + 1 = 5$. Thus, the mean free path for ω is given by

$$\frac{2a + a + a + 2a + a}{b(\omega) + 1} = \frac{7}{5}a. \quad (\text{S28})$$

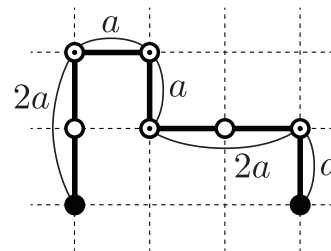


FIG. S4. Example configuration ω for $(n, r) = (7, 3a)$. The two endpoints are denoted by black circles (\bullet), and the bending points by circles with dots (\odot). The number of bending points $b(\omega)$ is four.

Because the numerator of the left-hand side of Eq. (S28) becomes na for an arbitrary ω , a mean free path can generally be rewritten as $na/(b(\omega) + 1)$ for an arbitrary n , the thermal average of which yielded Eq. (7) in the main text.

S10. SAW AND NAW LIMITS

The interacting SAW reduces to the SAW and NAW in the cases of $|\varepsilon| \ll k_B T$ and $\varepsilon \gg k_B T$, respectively. This section explains the SAW ($\varepsilon \rightarrow 0$) and NAW ($\varepsilon \rightarrow \infty$) limits of the interacting SAW, as shown in Fig. 5 in the main text.

A. Reduction to SAW ($\varepsilon \rightarrow 0$)

In the limit of $\varepsilon \rightarrow 0$, Eq. (3) in the main text becomes

$$Z(r, \infty) = \sum_{m=0}^{m_{\text{ub}}} W_{n,m}(r) = W_n(r), \quad (\text{S29})$$

because $\hat{T} \equiv k_B T/\varepsilon \rightarrow \infty$ and the Boltzmann factor becomes $e^{-m/\hat{T}} \rightarrow 1$ for each ω . This means that the interacting SAW reduces to the SAW, which is defined as an ensemble of equally weighted ω , in the limit of $\varepsilon \rightarrow 0$. Thus, we call this limit as the SAW limit.

In the SAW limit, $\hat{k}(r, \hat{T})/\hat{T}$ converges to the following finite value:

$$\lim_{\hat{T} \rightarrow \infty} \frac{\hat{k}(r, \hat{T})}{\hat{T}} = \left(\frac{\Delta W_n(r)}{Z(r, \infty) \Delta \hat{r}} \right)^2 - \frac{\Delta^2 W_n(r)}{Z(r, \infty) \Delta \hat{r}^2}. \quad (\text{S30})$$

For $(n, r) = (20, 10a)$, we obtain

$$\lim_{\hat{T} \rightarrow \infty} \frac{\hat{k}(10a, \hat{T})}{\hat{T}} = \frac{6313217099066886233}{6892128429997467904} \simeq 0.916, \quad (\text{S31})$$

which is displayed in the top panel of Fig. 5 (dashed light-blue line labeled with ‘‘SAW’’) in the main text.

As discussed in Sec. S5, $\hat{k}_U(r, \hat{T})$ converges, in the SAW limit, to a finite rational number $\hat{k}_{\hat{U}}^\infty(r, \hat{T})$ [Eq. (S15)], while Eq. (S30) shows that $\hat{k}(r, \hat{T}) \rightarrow \infty$. Thus, we have

$$\lim_{\hat{T} \rightarrow \infty} \frac{\hat{k}_U(r, \hat{T})}{\hat{k}(r, \hat{T})} = \lim_{\hat{T} \rightarrow \infty} \frac{k_U(r, \hat{T})}{k(r, \hat{T})} = 0, \quad (\text{S32})$$

which means that the stiffness does not have an energetic contribution, and the elasticity of the lattice polymer chain is solely governed by entropy in the SAW limit.

B. Reduction to NAW ($\varepsilon \rightarrow \infty$)

In the limit of $\varepsilon \rightarrow \infty$, Eq. (3) in the main text becomes

$$Z(r, 0) = W_{n,0}(r), \quad (\text{S33})$$

because $\hat{T} \equiv k_B T/\varepsilon \rightarrow 0$ and the Boltzmann factor becomes $e^{-m/\hat{T}} \rightarrow 0$, except for $m = 0$. This means that the interacting SAW reduces to the NAW [S14, S18, S19], which is defined as the SAW without first-neighbor contacts ($m = 0$), in the limit of $\varepsilon \rightarrow \infty$, and thus we call this limit the NAW limit.

In the NAW limit, $\hat{k}(r, \hat{T})/\hat{T}$ converges to the following finite value:

$$\lim_{\hat{T} \rightarrow 0} \frac{\hat{k}(r, \hat{T})}{\hat{T}} = \left(\frac{\Delta W_{n,0}(r)}{Z(r, 0) \Delta \hat{r}} \right)^2 - \frac{\Delta^2 W_{n,0}(r)}{Z(r, 0) \Delta \hat{r}^2}. \quad (\text{S34})$$

For $(n, r) = (20, 10a)$, we obtain

$$\lim_{\hat{T} \rightarrow 0} \frac{\hat{k}(10a, \hat{T})}{\hat{T}} = \frac{3389461192866292}{17118017290177281} \simeq 0.198, \quad (\text{S35})$$

which is displayed in the top panel of Fig. 5 (dashed yellow line labeled with ‘‘NAW’’) in the main text.

From Eq. (S14), the Taylor series of $\hat{k}_U(r, \hat{T})$ around $e^{-1/\hat{T}} = 0$ ($\hat{T} = 0$) is

$$\hat{k}_U(r, \hat{T}) = \left(\frac{\Delta^2 W_{n,1}}{W_{n,0} \Delta \hat{r}^2} - \frac{W_{n,1} \Delta^2 W_{n,0} + 2 \Delta W_{n,0} \Delta W_{n,1}}{W_{n,0}^2 \Delta \hat{r}^2} + \frac{2 W_{n,1} \Delta W_{n,0}^2}{W_{n,0}^3 \Delta \hat{r}^2} \right) e^{-1/\hat{T}} + O(e^{-2/\hat{T}}). \quad (\text{S36})$$

Equation (S36) means that $\hat{k}_U(r, \hat{T})$ decays exponentially in the NAW limit. By using Eqs. (S34) and (S36), we obtain

$$\lim_{\hat{T} \rightarrow 0} \frac{\hat{k}_U(r, \hat{T})}{\hat{k}(r, \hat{T})} = \lim_{\hat{T} \rightarrow 0} \frac{k_U(r, \hat{T})}{k(r, \hat{T})} = 0, \quad (\text{S37})$$

which means that the stiffness does not have an energetic contribution, and the elasticity of the lattice polymer chain is solely governed by entropy in the NAW limit.

S11. TABLES OF ENUMERATION RESULTS

We provide complete lists of $W_n(r)$ and $W_{n,m}(r)$ for $n = 1$ –20 in Tables S1–S19. We also provide a list of $W_{n,m}((n-8)a)$ in Table S20. Notably, each column in Tables S1–S20 has at least one value greater than 0. For $W_n(r) \geq 1$ (i.e., ω exists), $\hat{r} \equiv r/a$ is required to be odd in the case of odd n (see Table S1), and \hat{r} is required to be even in the case of even n (Table S2).

TABLE S1. List of $W_n(r)$ for $n = 1, 3, \dots, 19$. Values in column $W_n(a)$ are confirmed by Ref. [S6] and those in row $n = 13$ are confirmed by Ref. [S7].

n	r									
	a	$3a$	$5a$	$7a$	$9a$	$11a$	$13a$	$15a$	$17a$	$19a$
1	1	0	0	0	0	0	0	0	0	0
3	4	1	0	0	0	0	0	0	0	0
5	44	24	1	0	0	0	0	0	0	0
7	552	516	60	1	0	0	0	0	0	0
9	8040	8936	2320	112	1	0	0	0	0	0
11	127016	154752	61624	6944	180	1	0	0	0	0
13	2112320	2729100	1408808	272136	16452	264	1	0	0	0
15	36484128	49090288	29916784	8362224	903880	33484	364	1	0	0
17	648529392	898975960	614123820	221870344	36713772	2468712	61256	480	1	0
19	11790401800	16720159740	12409673296	5391815300	1222907256	129356500	5851096	103560	612	1

TABLE S2. List of $W_n(r)$ for $n = 2, 4, \dots, 20$.

n	r									
	$2a$	$4a$	$6a$	$8a$	$10a$	$12a$	$14a$	$16a$	$18a$	$20a$
2	1	0	0	0	0	0	0	0	0	0
4	12	1	0	0	0	0	0	0	0	0
6	184	40	1	0	0	0	0	0	0	0
8	2616	1172	84	1	0	0	0	0	0	0
10	40744	25180	4164	144	1	0	0	0	0	0
12	673040	497812	135232	10936	220	1	0	0	0	0
14	11563632	9562412	3587520	510516	23840	312	1	0	0	0
16	204708128	182639672	84977400	18088032	1524744	45804	420	1	0	0
18	3709636344	3496496500	1892115152	538054084	70560108	3858956	80332	544	1	0
20	68496828560	67289840344	40683432604	14322531084	2625286352	227589504	8638480	131504	684	1

We list $W_{n,m}(r)$ in Tables S3–S19. Because $W_{n,m}(r - \Delta r)$ and $W_{n,m}(r + \Delta r)$ for $\Delta r \equiv 2a$ are required to calculate the stiffness $\hat{k}(r, \hat{T})$, the minimum set of n and r that provides the analytic expression for $\hat{k}(r, \hat{T})$ is $(n, r) = (5, 3a)$, as shown in Table S4.

TABLE S4. List of $W_{n,m}(r)$ for $n = 5$.

m	r		
	a	$3a$	$5a$
0	0	12	1
1	8	12	0
2	36	0	0

TABLE S3. List of $W_{n,m}(r)$ for $n = 1-4$.

n	r	m	$W_{n,m}(r)$
1	a	0	1
2	$2a$	0	1
3	a	1	4
3	$3a$	0	1
4	$2a$	0	4
4	$2a$	1	8
4	$4a$	0	1

TABLE S5. List of $W_{n,m}(r)$ for $n = 6$.

m	r		
	$2a$	$4a$	$6a$
0	44	24	1
1	64	16	0
2	76	0	0

TABLE S6. List of $W_{n,m}(r)$ for $n = 7$.

m	r			
	a	$3a$	$5a$	$7a$
0	0	188	40	1
1	72	196	20	0
2	128	128	0	0
3	336	4	0	0
4	0	0	0	0
5	16	0	0	0

TABLE S10. List of $W_{n,m}(r)$ for $n = 11$.

m	r					
	a	$3a$	$5a$	$7a$	$9a$	$11a$
0	0	20160	18344	4024	144	1
1	9628	35924	23144	2324	36	0
2	20784	38940	13812	576	0	0
3	26112	32044	5392	20	0	0
4	22432	18564	848	0	0	0
5	33492	7248	84	0	0	0
6	9648	1440	0	0	0	0
7	4656	432	0	0	0	0
8	0	0	0	0	0	0
9	264	0	0	0	0	0

TABLE S7. List of $W_{n,m}(r)$ for $n = 8$.

m	r			
	$2a$	$4a$	$6a$	$8a$
0	364	520	60	1
1	688	440	24	0
2	724	204	0	0
3	688	8	0	0
4	120	0	0	0
5	32	0	0	0

TABLE S11. List of $W_{n,m}(r)$ for $n = 12$.

m	r					
	$2a$	$4a$	$6a$	$8a$	$10a$	$12a$
0	47104	77668	45512	6668	180	1
1	100400	133304	52240	3496	40	0
2	127652	131032	27332	748	0	0
3	133720	92360	8888	24	0	0
4	116140	45400	1156	0	0	0
5	87360	14296	104	0	0	0
6	43288	3032	0	0	0	0
7	12304	720	0	0	0	0
8	4656	0	0	0	0	0
9	416	0	0	0	0	0

TABLE S8. List of $W_{n,m}(r)$ for $n = 9$.

m	r				
	a	$3a$	$5a$	$7a$	$9a$
0	0	1836	1160	84	1
1	820	2868	844	28	0
2	1600	2392	304	0	0
3	1680	1448	12	0	0
4	3300	344	0	0	0
5	320	48	0	0	0
6	320	0	0	0	0

TABLE S9. List of $W_{n,m}(r)$ for $n = 10$.

m	r				
	$2a$	$4a$	$6a$	$8a$	$10a$
0	3976	6416	2264	112	1
1	7608	8944	1456	32	0
2	9408	6204	428	0	0
3	8960	2968	16	0	0
4	7376	584	0	0	0
5	2656	64	0	0	0
6	616	0	0	0	0
7	144	0	0	0	0

TABLE S12. List of $W_{n,m}(r)$ for $n = 13$.

m	r						
	a	$3a$	$5a$	$7a$	$9a$	$11a$	$13a$
0	0	237688	256604	101232	10460	220	1
1	120736	486628	418852	106240	5020	44	0
2	277200	581980	374616	49368	944	0	0
3	373548	557096	230512	13664	28	0	0
4	397656	435816	96336	1508	0	0	0
5	318696	256008	25636	124	0	0	0
6	363524	121020	5244	0	0	0	0
7	174104	38280	1008	0	0	0	0
8	66696	13112	0	0	0	0	0
9	12768	1120	0	0	0	0	0
10	7392	352	0	0	0	0	0

TABLE S19. List of $W_{n,m}(r)$ for $n = 20$.

m	r										
	$2a$	$4a$	$6a$	$8a$	$10a$	$12a$	$14a$	$16a$	$18a$	$20a$	
0	1452657120	2245560848	2172427044	1457206084	523343364	80444436	4730696	98884	612	1	
1	4204845176	6100416256	5550780112	3145134240	843385216	86762704	3030224	29576	72	0	
2	7031181480	9473908684	7864625864	3615527208	689830188	44243756	771684	2988	0	0	
3	9039457896	11195485032	8224333568	2940899072	377456344	13368784	100408	56	0	0	
4	9813883384	11012590952	6883346012	1813973596	142418328	2428036	5204	0	0	0	
5	9423021280	9392110424	4793131304	871249112	38702224	304096	264	0	0	0	
6	8201084228	7129076172	2822253972	334283424	8335124	34644	0	0	0	0	
7	6588653712	4859106768	1418261432	107410032	1577456	3048	0	0	0	0	
8	4923371532	2962292832	617683056	28987348	212612	0	0	0	0	0	
9	3389606120	1599350584	232706440	6459240	22680	0	0	0	0	0	
10	2159025216	783876948	76440080	1177344	2816	0	0	0	0	0	
11	1219978864	342570672	21220512	208176	0	0	0	0	0	0	
12	624337768	133619932	5137464	13904	0	0	0	0	0	0	
13	272912720	43748496	925824	2304	0	0	0	0	0	0	
14	108302496	12849536	145120	0	0	0	0	0	0	0	
15	33279056	2733696	14800	0	0	0	0	0	0	0	
16	9601392	484528	0	0	0	0	0	0	0	0	
17	1261536	57984	0	0	0	0	0	0	0	0	
18	367584	0	0	0	0	0	0	0	0	0	

TABLE S20. List of $W_{n,m}((n-8)a)$ for $n = 21-26$.

n	m							
	0	1	2	3	4	5	6	7
21	144322060	147779272	70634012	19763748	3294652	381840	40888	3340
22	249379884	242937552	109194420	28422200	4373480	471520	47644	3632
23	416838708	387090544	164111960	39902332	5696176	573952	54912	3924
24	676458552	599937040	240586012	54847968	7296548	689952	62692	4216
25	1069126256	907138184	344982036	73994724	9210556	820336	70984	4508
26	1649999040	1341596272	484996292	98176168	11476312	965920	79788	4800

S12. POLYNOMIAL FUNCTIONS $W_{n,m}((n-2)a)$, $W_{n,m}((n-4)a)$, $W_{n,m}((n-6)a)$, AND $W_{n,m}((n-8)a)$

This section presents the analytic expressions for $W_{n,m}((n-2)a)$, $W_{n,m}((n-4)a)$, $W_{n,m}((n-6)a)$, and $W_{n,m}((n-8)a)$.

For $r = na$, only the fully stretched ω is allowed, and thus

$$W_{n,0}(na) = 1 \quad (n \geq 1), \quad (\text{S38})$$

$$W_{n,m}(na) = 0 \quad (n \geq 1, m \geq 1). \quad (\text{S39})$$

Assuming that $W_{n,m}((n-2)a)$ and $W_{n,m}((n-4)a)$ are polynomial functions of n , their exact forms are calculated using the values in Tables S3–S19 as

$$W_{n,0}((n-2)a) = 2(n-2)(n-3) \quad (n \geq 2), \quad (\text{S40})$$

$$W_{n,1}((n-2)a) = 4(n-2) \quad (n \geq 2), \quad (\text{S41})$$

$$W_{n,m}((n-2)a) = 0 \quad (n \geq 0, m \geq 2), \quad (\text{S42})$$

$$W_{n,0}((n-4)a) = \frac{1}{2}(3n^4 - 50n^3 + 353n^2 - 1266n + 1888) \quad (n \geq 6), \quad (\text{S43})$$

$$W_{n,1}((n-4)a) = 4(2n^3 - 28n^2 + 143n - 266) \quad (n \geq 6), \quad (\text{S44})$$

$$W_{n,2}((n-4)a) = 4(3n^2 - 26n + 67) \quad (n \geq 6), \quad (\text{S45})$$

$$W_{n,3}((n-4)a) = 4(n-6) \quad (n \geq 6), \quad (\text{S46})$$

$$W_{n,m}((n-4)a) = 0 \quad (n \geq 1, m \geq 4). \quad (\text{S47})$$

We confirmed that all above equations produce the same values in Tables S3–S19 up to $n = 20$. We also confirmed them by additional enumeration results up to $n = 87$.

The polynomial functions of $W_{n,m}((n-6)a)$ are also calculated using the values in Tables S9–S19 as

$$W_{n,0}((n-6)a) = \frac{1}{9}(5n^6 - 183n^5 + 2999n^4 - 28461n^3 + 166160n^2 - 565248n + 865224) \quad (n \geq 10), \quad (\text{S48})$$

$$W_{n,1}((n-6)a) = 2(3n^5 - 98n^4 + 1367n^3 - 10236n^2 + 41244n - 71368) \quad (n \geq 10), \quad (\text{S49})$$

$$W_{n,2}((n-6)a) = 2(11n^4 - 289n^3 + 3018n^2 - 14966n + 29962) \quad (n \geq 10), \quad (\text{S50})$$

$$W_{n,3}((n-6)a) = \frac{8}{3}(13n^3 - 228n^2 + 1394n - 3027) \quad (n \geq 10), \quad (\text{S51})$$

$$W_{n,4}((n-6)a) = 2(11n^2 - 99n + 182) \quad (n \geq 10), \quad (\text{S52})$$

$$W_{n,5}((n-6)a) = 4(5n - 34) \quad (n \geq 10), \quad (\text{S53})$$

$$W_{n,m}((n-6)a) = 0 \quad (n \geq 1, m \geq 6). \quad (\text{S54})$$

We confirmed that all above equations yield the same values in Tables S9–S19 up to $n = 20$. We also confirmed them by extra enumeration results up to $n = 35$.

The polynomial functions of $W_{n,m}((n-8)a)$ are also calculated using the values in Tables S13–S20 as

$$W_{n,0}((n-8)a) = \frac{1}{288}(35n^8 - 2260n^7 + 67334n^6 - 1214200n^5 + 14548595n^4 - 118874980n^3 + 646859556n^2 - 2137772688n + 3268268928) \quad (n \geq 14), \quad (\text{S55})$$

$$W_{n,1}((n-8)a) = \frac{2}{9}(10n^7 - 596n^6 + 15931n^5 - 248384n^4 + 2448529n^3 - 15309446n^2 + 56305152n - 93884472) \quad (n \geq 14), \quad (\text{S56})$$

$$W_{n,2}((n-8)a) = \frac{2}{3}(23n^6 - 1184n^5 + 26420n^4 - 328445n^3 + 2412356n^2 - 9985286n + 18288954) \quad (n \geq 14), \quad (\text{S57})$$

$$W_{n,3}((n-8)a) = \frac{2}{3}(77n^5 - 3118n^4 + 51571n^3 - 437066n^2 + 1917102n - 3550464) \quad (n \geq 14), \quad (\text{S58})$$

$$W_{n,4}((n-8)a) = \frac{1}{3}(269n^4 - 7306n^3 + 66553n^2 - 191348n - 102132) \quad (n \geq 14), \quad (\text{S59})$$

$$W_{n,5}((n-8)a) = 8(17n^3 - 325n^2 + 1606n - 108) \quad (n \geq 14), \quad (\text{S60})$$

$$W_{n,6}((n-8)a) = 4(64n^2 - 1063n + 4321) \quad (n \geq 14), \quad (\text{S61})$$

$$W_{n,7}((n-8)a) = 4(73n - 698) \quad (n \geq 14), \quad (\text{S62})$$

$$W_{n,m}((n-8)a) = 0 \quad (n \geq 1, m \geq 8). \quad (\text{S63})$$

We confirmed that all above equations produce the same values in Tables S13–S20 up to $n = 26$. We also confirmed them by additional enumeration results up to $n = 31$.

S13. NEGATIVENESS OF \hat{k}_U

In this section, we demonstrate that $\hat{k}_U(r, \hat{T}) < 0$ for (A) $r = (n-2)a$ and $n \geq 7$, (B) $r = (n-4)a$ and $n \geq 10$, and (C) $r = (n-6)a$ and $n \geq 13$ in the case of positive finite \hat{T} , i.e., $0 < \hat{T} < \infty$.

A. Negativeness of $\hat{k}_U((n-2)a, \hat{T})$ for $n \geq 7$ and positive finite \hat{T}

This section shows $\hat{k}_U((n-2)a, \hat{T}) < 0$ for $n \geq 7$ and $0 < \hat{T} < \infty$. Using Eq. (S14) and $W_{n,m}(r)$ for $r = na$, $(n-2)a$, and $(n-4)a$ given in Sec. S12, we derive

$$\hat{k}_U((n-2)a, \hat{T}) = \frac{\sum_{m=1}^7 u_m^{(2)}(n) e^{-m/\hat{T}}}{Z((n-2)a, \hat{T})^3 \Delta \hat{r}^2}, \quad (\text{S64})$$

where

$$u_1^{(2)}(n) = -\frac{15}{2}n^9 + 269n^8 - 4353n^7 + 41736n^6 - \frac{521903}{2}n^5 + 1098783n^4 - 3089556n^3 + 5518880n^2 - 5584358n + 2400620, \quad (\text{S65})$$

$$u_2^{(2)}(n) = -76n^8 + 2420n^7 - 34308n^6 + 281984n^5 - 1462040n^4 + 4861908n^3 - 10030208n^2 + 11596568n - 5693008, \quad (\text{S66})$$

$$u_3^{(2)}(n) = -306n^7 + 8466n^6 - 102066n^5 + 692886n^4 - 2846496n^3 + 7027860n^2 - 9557376n + 5452560, \quad (\text{S67})$$

$$u_4^{(2)}(n) = -620n^6 + 14664n^5 - 147476n^4 + 802152n^3 - 2470312n^2 + 4035648n - 2677216, \quad (\text{S68})$$

$$u_5^{(2)}(n) = -656n^5 + 13104n^4 - 106256n^3 + 433424n^2 - 876896n + 681472, \quad (\text{S69})$$

$$u_6^{(2)}(n) = -336n^4 + 5616n^3 - 34752n^2 + 93504n - 87552, \quad (\text{S70})$$

$$u_7^{(2)}(n) = -64(n-2)(n-6)^2. \quad (\text{S71})$$

The sign of $\hat{k}_V((n-2)a, \hat{T})$ is determined by the signs of $u_m^{(2)}$ ($1 \leq m \leq 7$), because the denominator of Eq. (S64), i.e., $Z((n-2)a, \hat{T})^3 \Delta \hat{r}^2$, is positive for $n \geq 7$. Eqs. (S65)–(S71) show that the signs of all the highest order terms of $u_m^{(2)}$ ($1 \leq m \leq 7$) are negative, which means that the numerator of Eq. (S64), i.e., $\sum_{m=1}^7 u_m^{(2)}(n) e^{-m/\hat{T}}$, becomes negative for $n \geq n_{\max}^{(2)}$ and $0 < \hat{T} < \infty$. Here, $n_{\max}^{(2)}$ is the maximum real root of Eqs. (S65)–(S71). From Eq. (S65), we obtain $n_{\max}^{(2)} \simeq 6.059$. Thus, $\hat{k}_V((n-2)a, \hat{T}) < 0$ for $n \geq 7$ and $0 < \hat{T} < \infty$.

B. Negativeness of $\hat{k}_V((n-4)a, \hat{T})$ for $n \geq 10$ and positive finite \hat{T}

This section shows $\hat{k}_V((n-4)a, \hat{T}) < 0$ for $n \geq 10$ and $0 < \hat{T} < \infty$. Using Eq. (S14) and $W_{n,m}(r)$ for $r = (n-2)a$, $(n-4)a$, and $(n-6)a$ given in Sec. S12, we derive

$$\hat{k}_V((n-4)a, \hat{T}) = \frac{\sum_{m=1}^{13} u_m^{(4)}(n) e^{-m/\hat{T}}}{Z((n-4)a, \hat{T})^3 \Delta \hat{r}^2}, \quad (\text{S72})$$

where

$$u_1^{(4)} = \frac{1}{162} (-205n^{15} + 17363n^{14} - 698688n^{13} + 17730761n^{12} - 317419220n^{11} + 4245828881n^{10} - 43821416090n^9 + 355164512947n^8 - 2277397470243n^7 + 11544526951456n^6 - 45855780255442n^5 + 140117991125440n^4 - 318926398490256n^3 + 511004785243104n^2 - 516064526221536n + 247767166991232), \quad (\text{S73})$$

$$u_2^{(4)} = \frac{1}{81} (-2292n^{14} + 182962n^{13} - 6898709n^{12} + 162941603n^{11} - 2693619010n^{10} + 32962849596n^9 - 307814509095n^8 + 2227156036115n^7 - 12540489751504n^6 + 54667080390664n^5 - 181613304658406n^4 + 446081581133124n^3 - 766436668515864n^2 + 825222400134768n - 419988439723968), \quad (\text{S74})$$

$$u_3^{(4)} = \frac{1}{27} (-7519n^{13} + 558915n^{12} - 19501364n^{11} + 423083520n^{10} - 6368138721n^9 + 70212215259n^8 - 583211737640n^7 + 3694063829592n^6 - 17837621361724n^5 + 64846633975794n^4 - 172529312064648n^3 + 318184924389048n^2 - 364538996385120n + 195702377263488), \quad (\text{S75})$$

$$u_4^{(4)} = \frac{1}{27} (-43084n^{12} + 2943944n^{11} - 93752620n^{10} + 1840731370n^9 - 24817313664n^8 + 241999362864n^7 - 1749419009816n^6 + 9442153172062n^5 - 37743096655496n^4 + 108902191644560n^3 - 215118667552872n^2 + 260853620100048n - 146470815055296), \quad (\text{S76})$$

$$u_5^{(4)} = \frac{1}{27} (-160518n^{11} + 9936908n^{10} - 284229985n^9 + 4960184370n^8 - 58672327908n^7 + 493675756356n^6 - 3012574289145n^5 + 13317744068638n^4 - 41734540576604n^3 + 88117321096560n^2 - 112491169475760n + 65489934144960), \quad (\text{S77})$$

$$u_6^{(4)} = \frac{1}{9} \left(-138454n^{10} + 7648980n^9 - 193163868n^8 + 2936883228n^7 - 29757650838n^6 + 209746542876n^5 - 1039937635256n^4 + 3573849415860n^3 - 8124045206544n^2 + 10986555333456n - 6672578318208 \right), \quad (\text{S78})$$

$$u_7^{(4)} = \frac{1}{9} \left(-262602n^9 + 12793214n^8 - 281282902n^7 + 3664717478n^6 - 31169310400n^5 + 179313313244n^4 - 696829903744n^3 + 1760929607712n^2 - 2620070309760n + 1743666655104 \right), \quad (\text{S79})$$

$$u_8^{(4)} = \frac{1}{9} \left(-380812n^8 + 16233984n^7 - 307961064n^6 + 3400535688n^5 - 23925651852n^4 + 109883795592n^3 - 321827760272n^2 + 549918585792n - 420150423744 \right), \quad (\text{S80})$$

$$u_9^{(4)} = -47066n^7 + 1734106n^6 - 27881874n^5 + 254335006n^4 - 1424355060n^3 + 4904014744n^2 - 9624808720n + 8326067904, \quad (\text{S81})$$

$$u_{10}^{(4)} = \frac{1}{3} \left(-116020n^6 + 3601912n^5 - 47217340n^4 + 336098232n^3 - 1374987136n^2 + 3073310816n - 2941199808 \right), \quad (\text{S82})$$

$$u_{11}^{(4)} = \frac{1}{3} \left(-70024n^5 + 1820912n^4 - 19044392n^3 + 100891264n^2 - 272534112n + 300922368 \right), \quad (\text{S83})$$

$$u_{12}^{(4)} = -9840n^4 + 217872n^3 - 1797888n^2 + 6600768n - 9217536, \quad (\text{S84})$$

$$u_{13}^{(4)} = -64(n-6)(5n-34)^2. \quad (\text{S85})$$

The sign of $\hat{k}_U((n-4)a, \hat{T})$ is determined by the signs of $u_m^{(4)}$ ($1 \leq m \leq 13$), because the denominator of Eq. (S72), i.e., $Z((n-4)a, \hat{T})^3 \Delta \hat{r}^2$, is positive for $n \geq 10$. Eqs. (S73)–(S85) show that the signs of all the highest order terms of $u_m^{(4)}$ ($1 \leq m \leq 10$) are negative, which means that the numerator of Eq. (S64), i.e., $\sum_{m=1}^{13} u_m^{(4)}(n) e^{-m/\hat{T}}$, becomes negative for $n \geq n_{\max}^{(4)}$ and $0 < \hat{T} < \infty$. Here, $n_{\max}^{(4)}$ is the maximum real root of Eqs. (S73)–(S85). From Eq. (S73), we obtain $n_{\max}^{(4)} \simeq 9.376$. Thus, $\hat{k}_U((n-4)a, \hat{T}) < 0$ for $n \geq 10$ and $0 < \hat{T} < \infty$.

C. Negativeness of $\hat{k}_U((n-6)a, \hat{T})$ for $n \geq 13$ and positive finite \hat{T}

This section shows $\hat{k}_U((n-6)a, \hat{T}) < 0$ for $n \geq 13$ and $0 < \hat{T} < \infty$. Using Eq. (S14) and $W_{n,m}(r)$ for $r = (n-4)a$, $r = (n-6)a$, and $(n-8)a$ given in Sec. S12, we derive

$$\hat{k}_U((n-6)a, \hat{T}) = \frac{\sum_{m=1}^{19} u_m^{(6)}(n) e^{-m/\hat{T}}}{Z((n-6)a, \hat{T})^3 \Delta \hat{r}^2}, \quad (\text{S86})$$

where

$$u_1^{(6)} = \frac{1}{746496} \left(-22925n^{21} + 3651350n^{20} - 280572525n^{19} + 13839826100n^{18} - 491835217542n^{17} + 13394578705548n^{16} - 290258225825138n^{15} + 5128596084770864n^{14} - 75101845533459921n^{13} + 921314498644022870n^{12} - 9530979229274591217n^{11} + 83414456661395135244n^{10} - 617750432346814111772n^9 + 3860615533725157859096n^8 - 20237786401609541886192n^7 + 88105767039420150604160n^6 - 313715610584983672619328n^5 + 892634669763201915829632n^4 - 1957408417977989278040064n^3 + 3114100298779481453119488n^2 - 3206402212383458902425600n + 1606922746557142444277760 \right), \quad (\text{S87})$$

$$\begin{aligned}
u_2^{(6)} = \frac{1}{373248} & \left(-474725n^{20} + 72477575n^{19} - 5323156610n^{18} + 250183929702n^{17} - 8441916150108n^{16} \right. \\
& + 217454214304098n^{15} - 4437896193992216n^{14} + 73495640587216832n^{13} - 1003320446829472673n^{12} \\
& + 11404101758151396399n^{11} - 108541672144176036462n^{10} + 866834712312806494674n^9 \\
& - 5800838459693683585190n^8 + 32368042499535569509328n^7 - 149224276510783406184848n^6 \\
& + 560117593439229814433568n^5 - 1673174866998422091489120n^4 + 3837299622571001723063040n^3 \\
& - 6362231683063664156659200n^2 + 6804281931945297919598592n \\
& \left. - 3531205492848809083109376 \right), \tag{S88}
\end{aligned}$$

$$\begin{aligned}
u_3^{(6)} = \frac{1}{20736} & \left(-495875n^{19} + 72086460n^{18} - 5025247738n^{17} + 223394489829n^{16} \right. \\
& - 7102529220402n^{15} + 171653821513788n^{14} - 3271271052894104n^{13} + 50319169149151326n^{12} \\
& - 634158942279803035n^{11} + 6607661982448768920n^{10} - 57176346809850992550n^9 \\
& + 411032686072754768181n^8 - 2445957646395038035736n^7 + 11950350707040255519912n^6 \\
& - 47271964962020442274912n^5 + 148067212928307141442896n^4 - 354431490131617618928256n^3 \\
& \left. + 610754838651846303941376n^2 - 676280903480102933084160n + 362159556514847639764992 \right), \tag{S89}
\end{aligned}$$

$$\begin{aligned}
u_4^{(6)} = \frac{1}{20736} & \left(-5620285n^{18} + 772132941n^{17} - 50682756822n^{16} + 2113006447828n^{15} \right. \\
& - 62726107326294n^{14} + 1408503972817966n^{13} - 24801704091456024n^{12} + 350274467388318700n^{11} \\
& - 4023424777397486437n^{10} + 37880161507205000093n^9 - 293111471410540984602n^8 \\
& + 1860363913234590375512n^7 - 9617737330505538826208n^6 + 39973267634633782242512n^5 \\
& - 130711629673483090530080n^4 + 324730477367018637020160n^3 - 577635286547052572318208n^2 \\
& \left. + 657062120735043755065344n - 35996227069333721874432 \right), \tag{S90}
\end{aligned}$$

$$\begin{aligned}
u_5^{(6)} = \frac{1}{41472} & \left(-86374239n^{17} + 11118030894n^{16} - 680751301052n^{15} + 26345637587448n^{14} \right. \\
& - 722078681087354n^{13} + 14879005868088436n^{12} - 238754668762854404n^{11} + 3048069473546590952n^{10} \\
& - 31348779742809829039n^9 + 261261071604966089454n^8 - 1764566880882885053896n^7 \\
& + 9604722295689978919088n^6 - 41621561034169404074224n^5 + 140604985480011158758624n^4 \\
& - 357666125384940531806208n^3 + 645773077991961321868800n^2 - 739228426992453425504256n \\
& \left. + 404186906092371006947328 \right), \tag{S91}
\end{aligned}$$

$$\begin{aligned}
u_6^{(6)} = \frac{1}{216} & \left(-2519109n^{16} + 301054954n^{15} - 17019940109n^{14} + 604426476467n^{13} \right. \\
& - 15095427145153n^{12} + 281172547605099n^{11} - 4040360987784411n^{10} + 45680526525048917n^9 \\
& - 410503399138529674n^8 + 2939888305754964247n^7 - 16706993064096336872n^6 \\
& + 74441420566390517484n^5 - 254437714984828683168n^4 + 643073952504833286432n^3 \\
& \left. - 1128767985081512244864n^2 + 1221712905468316713984n - 608149305930026566656 \right), \tag{S92}
\end{aligned}$$

$$\begin{aligned}
u_7^{(6)} = \frac{1}{648} & \left(-32756323n^{15} + 3607145648n^{14} - 186648376466n^{13} + 6020529786436n^{12} \right. \\
& - 135370208237880n^{11} + 2246572148940090n^{10} - 28405848149145284n^9 + 278273548599611260n^8 \\
& - 2124940856914580017n^7 + 12606389734008460634n^6 - 57328372730768167542n^5 \\
& + 194569629878650336716n^4 - 469855782171501542952n^3 + 739277388220218599088n^2 \\
& \left. - 628430759332455883968n + 160520919782147767296 \right), \tag{S93}
\end{aligned}$$

$$\begin{aligned}
u_8^{(6)} = \frac{1}{648} & \left(-116440367n^{14} + 11779763789n^{13} - 556037454843n^{12} + 16231347437467n^{11} \right. \\
& - 327255408288211n^{10} + 4817510908935999n^9 - 53328847399804225n^8 + 449976144865454749n^7 \\
& - 2897724989746956462n^6 + 14088956084126042156n^5 - 50397048291189084356n^4 \\
& + 126197591177892469200n^3 - 200757496958428129488n^2 + 161745657184397195712n \\
& \left. - 23858838506519788032 \right), \tag{S94}
\end{aligned}$$

$$\begin{aligned}
u_9^{(6)} = \frac{1}{72} & \left(-39449002n^{13} + 3671864639n^{12} - 158499153965n^{11} + 4203519175384n^{10} \right. \\
& - 76458728456214n^9 + 1007702453590959n^8 - 9903811141683077n^7 + 73500501112531654n^6 \\
& - 411864338108951494n^5 + 1720428809657422244n^4 - 5203310623522143240n^3 \\
& \left. + 10775222610142696272n^2 - 13658680985546304576n + 7963232487942859776 \right), \tag{S95}
\end{aligned}$$

$$\begin{aligned}
u_{10}^{(6)} = \frac{1}{108} & \left(-156836388n^{12} + 13422268873n^{11} - 529491083274n^{10} + 12751566309959n^9 \right. \\
& - 209201009835930n^8 + 2468825217441915n^7 - 21547960824813174n^6 + 140593197746717825n^5 \\
& - 683107973403606858n^4 + 2420733604571102548n^3 - 5967244349696783544n^2 + 9232367726463329376n \\
& \left. - 6809357484417268224 \right), \tag{S96}
\end{aligned}$$

$$\begin{aligned}
u_{11}^{(6)} = \frac{1}{72} & \left(-237415031n^{11} + 18513703473n^{10} - 659368462582n^9 + 14185093823038n^8 \right. \\
& - 205315602729831n^7 + 2105539038681241n^6 - 15664778769980476n^5 + 84883702466085928n^4 \\
& - 329809005388563632n^3 + 879667384846802256n^2 - 1458163614590797248n \\
& \left. + 1145237089233286656 \right), \tag{S97}
\end{aligned}$$

$$\begin{aligned}
u_{12}^{(6)} = \frac{1}{12} & \left(-76017017n^{10} + 5325037344n^9 - 167894082086n^8 + 3140374045696n^7 - 38628157495073n^6 \right. \\
& + 326783899052848n^5 - 1926419437175376n^4 + 7811811918869872n^3 - 20825643072250992n^2 \\
& \left. + 32878321047905856n - 23272624228564224 \right), \tag{S98}
\end{aligned}$$

$$\begin{aligned}
u_{13}^{(6)} = \frac{1}{9} & \left(-93866834n^9 + 5858628640n^8 - 161643126752n^7 + 2585639077156n^6 - 26383735512470n^5 \right. \\
& + 177480372403756n^4 - 781186773484440n^3 + 2134445192018064n^2 - 3163028481951648n \\
& \left. + 1737395413622208 \right), \tag{S99}
\end{aligned}$$

$$\begin{aligned}
u_{14}^{(6)} = \frac{1}{9} & \left(-135337400n^8 + 7556760704n^7 - 183598113112n^6 + 2536829481800n^5 - 21820249213168n^4 \right. \\
& \left. + 119680667774120n^3 - 408247985819312n^2 + 787623607261920n - 648632386240704 \right), \tag{S100}
\end{aligned}$$

$$\begin{aligned}
u_{15}^{(6)} = & -18486076n^7 + 922340348n^6 - 19684120052n^5 + 233814892852n^4 - 1678620044832n^3 + 7335440548704n^2 \\
& - 18210926298720n + 19960569475392, \tag{S101}
\end{aligned}$$

$$\begin{aligned}
u_{16}^{(6)} = & -17558536n^6 + 762236576n^5 - 13720599480n^4 + 131631126624n^3 - 714423668032n^2 + 2098590900128n \\
& - 2635200769344, \tag{S102}
\end{aligned}$$

$$\begin{aligned}
u_{17}^{(6)} = \frac{1}{3} & \left(-34417792n^5 + 1247212336n^4 - 17748700224n^3 + 123907713968n^2 - 424390789856n \right. \\
& \left. + 570898285824 \right), \tag{S103}
\end{aligned}$$

$$u_{18}^{(6)} = -5056272n^4 + 153070320n^3 - 1694712576n^2 + 8104545984n - 14100627456, \tag{S104}$$

$$u_{19}^{(6)} = -(320n - 2176)(73n - 698)^2. \tag{S105}$$

The sign of $\hat{k}_U((n-6)a, \hat{T})$ is determined by the signs of $u_m^{(6)}$ ($1 \leq m \leq 19$), because the denominator of Eq. (S86), i.e., $Z((n-6)a, \hat{T})^3 \Delta \hat{r}^2$, is positive for $n \geq 1$. Eqs. (S87)–(S105) show that the signs of all the highest order terms of $u_m^{(6)}$ ($1 \leq m \leq 19$) are negative, which means that the numerator of Eq. (S64), i.e., $\sum_{m=1}^{19} u_m^{(6)}(n) e^{-m/\hat{T}}$, becomes negative for $n \geq n_{\max}^{(6)}$. Here, $n_{\max}^{(6)}$ is the maximum real root of Eqs. (S87)–(S105). From Eq. (S87), we obtain $n_{\max}^{(6)} \simeq 12.185$. Thus, $\hat{k}_U((n-6)a, \hat{T}) < 0$ for $n \geq 13$ and $0 < \hat{T} < \infty$.

S14. EXACT VALUES OF $\hat{T}_U^\infty(n, r)$ FOR $n = 5-20$

Tables S21–S22 list the exact rational numbers of $\hat{T}_U^\infty(n, r)$ calculated using Eq. (S17) with Tables S3–S19.

TABLE S21. List of $\hat{T}_U^\infty(n, r)$ for $n = 5-10$.

n	r	$\hat{T}_U^\infty(n, r)$
5	$3a$	$-489/2137$
6	$4a$	$147724/83445$
7	$3a$	$-797030/993429$
7	$5a$	$3382/2487$
8	$4a$	$26799212/86839633$
8	$6a$	$7547916/7234927$
9	$3a$	$-4055477596/5257358209$
9	$5a$	$152081266/83730105$
9	$7a$	$7611583/8876610$
10	$4a$	$-8701767992/21214395505$
10	$6a$	$40743141476/22363017045$
10	$8a$	$100085804/135876753$

TABLE S22. List of $\hat{T}_U^\infty(n, r)$ for $n = 11-20$.

n	r	$\hat{T}_U^\infty(n, r)$
11	3a	-519108885655/747047679378
11	5a	150299594390/186104580139
11	7a	50907107187/33152857465
11	9a	141364782/217320245
12	4a	-107927914267969/214649579344095
12	6a	105098983928149/57132219401028
12	8a	1472725414430/1132883874063
12	10a	142035836/242741103
13	3a	-49542736363607596/76900856671970925
13	5a	2640777994418116/55052813460174941
13	7a	238175247802385/122518857472329
13	9a	77953640267/69208879293
13	11a	406053479/761455803
14	4a	-1711574042333777273/4026857160711375875
14	6a	159995627194416533/141370347617653980
14	8a	163155707441654/93528121329711
14	10a	20053990443149/20128254326290
14	12a	3440746572/7011200365
15	3a	-96951623341841992793/150612777410131461334
15	5a	-691658064075583271/3549165818096600912
15	7a	70379027228440564/37327326576896655
15	9a	98381872135352663/64329495834135005
15	11a	330017198802136/368428513985895
15	13a	3419428382/7513919679
16	4a	-8091159753821109779690/24813727716071921292827
16	6a	17538926733215035378/36773165966476328825
16	8a	3298580625991134887/1630566022898346198
16	10a	46391532219242110/34342463654294913
16	12a	133661491866764/163885539932895
16	14a	12880467404/30335604135
17	3a	-9215486325414340895326952/13527245403641865728741155
17	5a	-41809822325295311362381/192527521747950888257130
17	7a	44666861266339617682797/32415542874022716503150
17	9a	3527424314659253062003/1862575181539491665133
17	11a	3426603000355700279/2835203948241401283
17	13a	38082280733740/50775263002529
17	15a	1158351747/2909123828
18	4a	-76832528089170214024094608/310877703447823092206324125
18	6a	445196997853554956285398/3167926616427454319937167
18	8a	22990244319620867204775960/11853824125949561633799469
18	10a	27085099971224902449460/15824987199150503783871
18	12a	16484600814607277895/15059491967623573226
18	14a	11954485092575332/17194567028030343
18	16a	40040228716/106770751497
19	3a	-9988624331188492916121307208/13462710041939624756480714205
19	5a	-526333026059559368350597412/3183878298414896098809548197
19	7a	8969653836538056085422828/10733029537802793740799805
19	9a	10433146285561695510721997/5035720958544970805424924
19	11a	15253443674321829101249/9896772845670121649875
19	13a	638884010258507888779/637690480464228768091
19	15a	16736774506909468/25800961782825345
19	17a	33417089806/94265509545
20	4a	-156424594388085304183446401308/800126304549386100628524904191
20	6a	5654841561860857134828147888/351604494886093084914378540151
20	8a	213064242332431581643738876912/136140083511165456790525659591
20	10a	2060069205296200981486403946/1035875167962083022664474501
20	12a	23576578880315259956969/16889350416398519119800
20	14a	17349414652636502449/18755572078860566465
20	16a	21945750789458799/36063701991448955
20	18a	108187482924/321802699363

S15. RATIONAL FUNCTIONS $\hat{T}_U^\infty(n, (n-2)a)$, $\hat{T}_U^\infty(n, (n-4)a)$, AND $\hat{T}_U^\infty(n, (n-6)a)$

This section shows the analytic expressions for $\hat{T}_U^\infty(n, (n-2)a)$, $\hat{T}_U^\infty(n, (n-4)a)$, and $\hat{T}_U^\infty(n, (n-6)a)$. Using $W_{n,m}(na)$, $W_{n,m}((n-2)a)$, $W_{n,m}((n-4)a)$, $W_{n,m}((n-6)a)$, and $W_{n,m}((n-8)a)$ given in Sec. S12, we can derive the following rational functions:

$$\hat{T}_U^\infty(n, (n-2)a) = \frac{4p_2(n)}{(n-1)q_2(n)}, \quad (\text{S106})$$

$$\hat{T}_U^\infty(n, (n-4)a) = \frac{4p_4(n)}{(n-4)(3n^3 - 22n^2 + 65n - 62)q_4(n)}, \quad (\text{S107})$$

$$\hat{T}_U^\infty(n, (n-6)a) = \frac{4p_6(n)}{(5n^6 - 129n^5 + 1433n^4 - 8745n^3 + 30962n^2 - 60390n + 49320)q_6(n)}, \quad (\text{S108})$$

where

$$\begin{aligned} p_2(n) &= 15n^8 - 356n^7 + 3766n^6 - 23016n^5 + 88019n^4 - 213804n^3 + 317784n^2 - 256008n + 81484, \\ q_2(n) &= 9n^8 - 204n^7 + 2026n^6 - 11648n^5 + 42733n^4 - 102444n^3 + 156272n^2 - 137656n + 53028, \\ p_4(n) &= 205n^{15} - 12779n^{14} + 377878n^{13} - 7028329n^{12} + 91843642n^{11} - 891705537n^{10} + 6632586110n^9 \\ &\quad - 38412484159n^8 + 174308221229n^7 - 618529465700n^6 + 1698600661640n^5 - 3535919882472n^4 \\ &\quad + 5382532241712n^3 - 5629298377824n^2 + 3590676428544n - 1040974789248, \\ q_4(n) &= 25n^{12} - 1290n^{11} + 30701n^{10} - 447138n^9 + 4450497n^8 - 31949658n^7 + 169814699n^6 \\ &\quad - 673658250n^5 + 1979577382n^4 - 4199479272n^3 + 6095057184n^2 - 5417182800n + 2218551120, \\ p_6(n) &= 22925n^{21} - 2701900n^{20} + 153468875n^{19} - 5586295180n^{18} + 146134227132n^{17} - 2919787308972n^{16} \\ &\quad + 46223429811614n^{15} - 593623263577288n^{14} + 6280555247726285n^{13} - 55286737479509908n^{12} \\ &\quad + 407269495940367735n^{11} - 2516577055829714988n^{10} + 13034676945473036810n^9 - 56377142495508236116n^8 \\ &\quad + 202149359931692608736n^7 - 594051500342010659680n^6 + 1406389826610734976288n^5 \\ &\quad - 2614817373934251716928n^4 + 3671888987236959830016n^3 - 3653905354412312687616n^2 \\ &\quad + 2288827258144328171520n - 675038669997797867520, \\ q_6(n) &= 1225n^{16} - 113400n^{15} + 4954420n^{14} - 135769920n^{13} + 2614686966n^{12} - 37554353328n^{11} + 416423467068n^{10} \\ &\quad - 3638603477568n^9 + 25331854157561n^8 - 141042593225496n^7 + 626123307241416n^6 - 2193065510167104n^5 \\ &\quad + 5940674302476560n^4 - 12025282548916608n^3 + 17136895425944832n^2 - 15333010803855360n \\ &\quad + 647058547775360. \end{aligned}$$

We confirmed that Eqs. (S106), (S107), and (S108) provide the correct rational numbers, as listed in Tables S21 and S22, for $5 \leq n \leq 20$. We also confirmed that Eq. (S106) yields the correct rational numbers up to $n = 80$, Eq. (S107) up to $n = 35$, and Eq. (S108) up to $n = 31$, based on additional exact enumeration results.

-
- [S1] W. J. Orr, Statistical treatment of polymer solutions at infinite dilution, *Trans. Faraday Soc.* **43**, 12 (1947).
[S2] Y. H. Hsieh, C. N. Chen, and C. K. Hu, Efficient algorithm for computing exact partition functions of lattice polymer models, *Comput. Phys. Commun.* **209**, 27 (2016).
[S3] R. D. Schram, G. T. Barkema, and R. H. Bisseling, Exact enumeration of self-avoiding walks, *J. Stat. Mech.* (2011) P06019.
[S4] R. D. Schram, G. T. Barkema, and R. H. Bisseling, SAWdoubler: A program for counting self-avoiding walks, *Comput. Phys. Commun.* **184**, 891 (2013).
[S5] N. Clisby, R. Liang, and G. Slade, Self-avoiding walk enumeration via the lace expansion, *J. Phys. A* **40**, 10973 (2007).
[S6] P. Butera and M. Comi, Critical specific heats of the N-vector spin models on the simple cubic and bcc lattices, *Phys. Rev. B* **60**, 6749 (1999).
[S7] C. Domb, J. Gillis, and G. Wilmers, On the shape and configuration of polymer molecules, *Proc. Phys. Soc. London* **85**, 625 (1965).
[S8] M. E. Fisher and M. F. Sykes, Excluded-volume problem and the Ising model of ferromagnetism, *Phys. Rev.* **114**, 45 (1959).
[S9] M. F. Sykes, Some counting theorems in the theory of the Ising model and the excluded volume problem,

- J. Math. Phys.* **2**, 52 (1961).
- [S10] M. F. Sykes, Self-avoiding walks on the simple cubic lattice, *J. Chem. Phys.* **39**, 410 (1963).
- [S11] A. J. Guttmann, On the critical behaviour of self-avoiding walks, *J. Phys. A* **20**, 1839 (1987).
- [S12] N. J. A. Sloane, Entry A001412 in The On-Line Encyclopedia of Integer Sequences, <https://oeis.org/A001412> (2022).
- [S13] M. E. Fisher and B. J. Hiley, Configuration and free energy of a polymer molecule with solvent interaction, *J. Chem. Phys.* **34**, 1253 (1961).
- [S14] A. M. Nemirovsky, K. F. Freed, T. Ishinabe, and J. F. Douglas, Marriage of exact enumeration and $1/d$ expansion methods: Lattice model of dilute polymers, *J. Stat. Phys.* **67**, 1083 (1992).
- [S15] J. Myers, Entry A174319 in The On-Line Encyclopedia of Integer Sequences, <https://oeis.org/A174319> (2022).
- [S16] B. Nienhuis, Exact Critical Point and Critical Exponents of $O(n)$ Models in Two Dimensions, *Phys. Rev. Lett.* **49**, 1062 (1982).
- [S17] B. Nienhuis, Critical behavior of two-dimensional spin models and charge asymmetry in the Coulomb gas, *J. Stat. Phys.* **34**, 731 (1984).
- [S18] G. Torrie and S. G. Whittington, Exact enumeration of neighbour-avoiding walks on the tetrahedral and body-centred cubic lattices, *J. Phys. A* **8**, 1178 (1975).
- [S19] T. Ishinabe and Y. Chikahisa, Exact enumerations of self-avoiding lattice walks with different nearest-neighbor contacts, *J. Chem. Phys.* **85**, 1009 (1986).